A Multiscale Investigation of Repolarization Variability and Its Role in Cardiac Arrhythmogenesis

Esther Pueyo,[†‡§*] Alberto Corrias,[†] László Virág,[¶] Norbert Jost,[‖] Tamás Szél,[¶] András Varró,[¶‖] Norbert Szentandrássy,[**] Péter P. Nánási,[**] Kevin Burrage,[†] and Blanca Rodríguez[†]

[†]Department of Computer Science, University of Oxford, Oxford, United Kingdom; [‡]Aragón Institute of Engineering Research, IIS Aragón, Universidad de Zaragoza, Zaragoza, Spain; [§]Biomedical Research Networking Center in Bioengineering, Biomaterials and Nanomedicine, Zaragoza, Spain; [¶]Department of Pharmacology and Pharmacotherapy, University of Szeged, Szeged, Hungary; [‖]Division of Cardiovascular Pharmacology, Hungarian Academy of Sciences, Szeged, Hungary; and **Department of Physiology, University of Debrecen, Debrecen, Hungary

ABSTRACT Enhanced temporal and spatial variability in cardiac repolarization has been related to increased arrhythmic risk both clinically and experimentally. Causes and modulators of variability in repolarization and their implications in arrhythmogenesis are however not well understood. At the ionic level, the slow component of the delayed rectifier potassium current (I_{Ks}) is an important determinant of ventricular repolarization. In this study, a combination of experimental and computational multiscale studies is used to investigate the role of intrinsic and extrinsic noise in I_{Ks} in modulating temporal and spatial variability in ventricular repolarization in human and guinea pig. Results show that under physiological conditions: i), stochastic fluctuations in I_{Ks} gating properties (i.e., intrinsic noise) cause significant beat-to-beat variability in action potential duration (APD) in isolated cells, whereas cell-to-cell differences in channel numbers (i.e., extrinsic noise) also contribute to cell-to-cell APD differences; ii), in tissue, electrotonic interactions mask the effect of I_{Ks} noise, resulting in a significant decrease in APD temporal and spatial variability compared to isolated cells. Pathological conditions resulting in gap junctional uncoupling or a decrease in repolarization reserve uncover the manifestation of I_{Ks} noise at cellular and tissue level, resulting in enhanced ventricular variability and abnormalities in repolarization such as afterdepolarizations and alternans.

INTRODUCTION

A large body of research has tried to unravel the mechanisms of lethal arrhythmias. However, the reasons why a particular patient dies on a particular day still remain a mystery. Different hearts can exhibit a very different response to a similar trigger, some developing arrhythmias, whereas others remain in sinus rhythm. Moreover, the same heart and even the same cell can react differently to a similar trigger at different times due to temporal variability and stochastic events. Enhanced temporal and spatial variability in cardiac repolarization has been linked to increased arrhythmic risk in both experimental (1–3) and clinical studies (4,5). The causes of spatiotemporal cardiac repolarization variability are still under investigation but are likely to involve complex multiscale mechanisms from the ionic to the whole organ level.

This study aims at investigating causes and modulators of temporal and spatial variability in ventricular repolarization using a combined experimental and computational approach. On the basis of previous experimental findings (6,7), we hypothesize that fluctuations in ionic currents caused by stochasticity in ion channel behavior contribute to variability in cardiac repolarization, particularly under pathological conditions. We also postulate that electrotonic interactions through intercellular coupling act to mitigate spatiotemporal variability in repolarization dynamics in tissue, as compared to isolated cells. Our study specifically focuses on investigating the role that stochasticity in the slow component of the delayed rectifier potassium current (I_{Ks}) plays in modulating variability in ventricular repolarization in human and guinea pig. Among all ionic currents, the slow kinetics and small channel numbers associated with I_{Ks} are likely to result in larger stochastic ionic current fluctuations compared to other currents with larger channel numbers and, consequently, reduced fluctuations. Furthermore, I_{Ks} has been shown to be an important determinant of repolarization stability, especially under reduced repolarization reserve conditions (3,8). Stochasticity in I_{Ks} has also been shown to determine beating rate irregularity in embryonic chick cells (9).

Our approach to investigate the implications of I_{Ks} stochasticity in repolarization variability combines experimental and computational investigations in human and guinea pig. Multiscale stochastic models of ventricular electrophysiology are developed, bridging ion channel numbers to whole organ behavior. Intrinsic (random gating) and extrinsic (cell-to-cell differences) noises in I_{Ks} are included in the models based on experimental data at different scales. Intrinsic noise properties are modeled using a stochastic differential equation (SDE) of Langevin type driven by Wiener noise (10), rather than using discrete Markov processes, for computational efficiency (11). Models are thoroughly validated by comparing simulated and experimental results on ionic current, cellular, tissue, and electrocardiogram (ECG) properties.

Submitted May 2, 2011, and accepted for publication September 27, 2011.

*Correspondence: epueyo@unizar.es

Editor: Andrew McCulloch.

0006-3495/11/12/2892/11 $2.00

doi: 10.1016/j.bpj.2011.09.060

There are a number of studies in the literature that have modeled the stochastic behavior of cardiac ion channels using different methodological approaches, e.g., by adding a global fluctuation current (12), by determining the state and lifetimes of channel gates (6), or by using SDEs (13). To the best of our knowledge, four previous studies have included a stochastic I_{Ks} formulation in ventricular models. Sato et al. (14) introduced a stochastic Langevin equation to describe I_{Ks} gating dynamics in a rabbit ventricular action potential (AP) model. Their formulation was, however, not based on experimental data, thus limiting the conclusions about fluctuation-induced effects at higher levels. Krogh-Madsen (9) developed a stochastic model of embryonic chick ventricular cells with a mathematical formulation of I_{Ks} stochastic gating, and Silva et al. (15) combined molecular structural dynamics with electrophysiological modeling to describe I_{Ks}, but no investigation was conducted in those two studies on the role of I_{Ks} stochasticity in modulating spatiotemporal variability in repolarization and its link to proarrhythmia, which are major objectives of this study. A very recent work published by Lemay et al. (16) shares these objectives with our study. However, while the paper by Lemay et al., as well as a preliminary work already presented by our group (17), both present a purely computational investigation, this study uses specific experimental data both for the development of the stochastic AP models and for confirmation of simulation predictions. Furthermore, two different species, i.e., guinea pig and human, are investigated in our study, and experimental and computational data are provided to show the validity of the results in the two species. Lemay et al. use a guinea pig model and develop stochastic formulations for different ionic currents based on experimental data from the literature corresponding to a range of different species, including rat, human, or guinea pig.

MATERIALS AND METHODS

Stochastic cell and tissue models

I_{Ks} stochastic gating was simulated by introducing intrinsic noise into two mathematical AP models, namely the human ten Tusscher-Panfilov (TP06) (18) and the guinea pig Faber-Rudy (FR07) (19). In both models, the Hodgkin-Huxley formulation for the I_{Ks} gating variables was replaced by a novel formulation based on the Langevin equation (20). In the case of the TP06 model, the ordinary differential equation defining the gating variable x_s,

$$dx_s = \frac{x_{s\infty}(V) - x_s}{\tau_{xs}(V)}dt, \tag{1}$$

was replaced by the following SDE:

$$dx_s = \frac{x_{s\infty}(V) - x_s}{\tau_{xs}(V)}dt + \frac{1}{(\tau_{xs}(V)n_{Ks})^{\frac{1}{2}}}(x_{s\infty}(V) + (1 - 2x_{s\infty}(V))x_s)^{\frac{1}{2}}dW, \tag{2}$$

where V is the transmembrane voltage, $x_{s\infty}$ and τ_{xs} are the steady-state value of x_s and the time constant to reach that steady-state value (both being functions of V), n_{Ks} is the number of I_{Ks} channels in the cell membrane, and W represents a Wiener process. In the case of the FR07 model, SDEs analogous to Eq. 2 were formulated for the two I_{Ks} gating variables x_{s1} and x_{s2}. As n_{Ks} becomes large, fluctuations in x_s introduced by the Wiener increment dW in Eq. 2 are decreased in magnitude, and the SDE is reduced to the standard ordinary differential equation of the TP06 model shown in Eq. 1 (analogously for the FR07 model).

Extrinsic noise was also included in the investigations by incorporating cell-to-cell differences in the number of I_{Ks} channels (n_{Ks}). Briefly, n_{Ks} was obtained from a truncated Gaussian distribution with mean m_n and standard deviation σ_n. The mean m_n was taken as the estimated n_{Ks} value derived as described in the Noise analysis subsection, whereas the standard deviation σ_n was computed as one-half of m_n to match the dispersion values obtained from experimental I_{Ks} current data, as described in the Supporting Material. The truncation of the Gaussian distribution was defined to set bounds on n_{Ks} that guaranteed that physiologically plausible AP durations were always obtained in the simulations (see the Supporting Material).

Transmural heterogeneities in the densities of I_{Ks} and I_{to} (transient outward potassium current) were introduced as in previous studies (18,21). A monodomain reaction-diffusion equation was used to model the propagation of the cellular APs in a transmural one-dimensional (1D) fiber and a ventricular mesh (22). Pseudo-ECG (extracellular unipolar potential) traces were computed as in (21), and were delineated using a wavelet-based system. Three stimulation protocols (periodic, decelerating frequency change, and dynamic restitution) were applied in single cell and tissue simulations. Further details are provided in the Supporting Material.

Experimental data

Experimental I_{Ks} current traces

Ventricular myocytes were enzymatically isolated from undiseased human donor hearts. Nisoldipine (1 mM) was used to block I_{CaL} (L-type calcium current), and E-4031 (1–5 μM) to inhibit I_{Kr} (rapid delayed rectifier potassium current). I_{Ks} currents were recorded with Axopatch-1D and Axopatch-200B patch-clamp amplifiers (Axon Instruments, Foster City CA) using the whole-cell configuration of the patch-clamp technique, and were digitized using a 333 kHz analog-to-digital converter (Digidata 1200, Axon Instruments). Low-pass filtering at 1 kHz was applied. Experiments were performed at 37°C.

Experimental APs in single myocytes

Dog and human. Ventricular myocytes were enzymatically isolated from dog and human hearts. Transmembrane potentials were recorded using 3 M KCl-filled sharp glass microelectrodes connected to the input of an Axoclamp-2B amplifier (Axon Instruments). The cells were paced at 1 Hz using 1-ms current pulses with 120% threshold amplitude. For drug experiments, an incubation period of 5–6 min was applied to develop the steady-state drug effect. APs were digitized at 200 kHz using Digidata 1200 A/D card (Axon Instruments).

Guinea pig. Ventricular myocytes were enzymatically isolated from guinea pig hearts, corresponding to the left ventricle base and apex subendo and subepicardial regions. The cell membrane potential was measured with the perforated patch method. The cells were paced at 1 Hz using 0.3-ms current pulses with 18 ± 2 nA amplitude. APs were digitized at 10 kHz, with a 5 kHz low-pass Bessel filter.

All experiments were performed at 37°C.

Experimental APs in tissue

Dog. Hearts were immediately removed from anesthetized adult mongrel dogs and rinsed in oxygenated Locke's solution at 37°C. Midmyocardial ventricular preparations were stimulated at 1 Hz using 2-ms voltage pulses twice diastolic threshold in amplitude.

Human. Human cardiac tissue was stored in cardioplegic solution at 4°C for 4–8 h, and papillary muscles were obtained from the right ventricle.

Preparations were stimulated at 1 Hz and were continuously superfused with Locke's solution. All experiments were performed at 37°C. Transmembrane potentials were recorded using conventional microelectrode technique.

For drug experiments, an incubation period of 60 min was applied to develop the steady-state drug effect.

Experiment approval by review boards

The human experimental protocol complied with the Declaration of World Medical Association proclaimed in Helsinki and was approved by the Ethical Review Board of the Albert Szent-Györgyi Medical University (No. 51-57/1997 OEj) and by the Scientific and Research Ethical Committee of the Medical Scientific Board at the Hungarian Ministry of Health (ETT-TUKEB), under ethical approval No. 4991-0/2010-1018EKU (339/PI/010). The guinea pig experiments were carried out in accordance with the UK Home Office guidance on the Operation of Animals (Scientific Procedures) Act of 1986. The dog experiments were carried out in compliance with the Guide for the Care and Use of Laboratory Animals (National Institutes of Health publication No. 85-23, revised 1985), and the protocols were approved by the Department of Animal Health and Food Control of the Ministry of Agriculture and Rural Development, Hungary (15.1/01031/006/2008).

More details about the experimental data and methods used in this study can be found in the Supporting Material.

Noise analysis

Fluctuation analysis of experimental and simulated macroscopic current measurements was applied to estimate the parameters required to model stochastic I_{Ks} fluctuations in human and guinea pig. We assumed n_{Ks} channels to gate independently and the current through each individual channel in any state to be either zero or the unitary current (i_{Ks}). Then, the following relationship between the variance σ_{Ks}^2 and the mean m_{Ks} of the macroscopic I_{Ks} current holds (23):

$$\sigma_{Ks}^2 = m_{Ks}\ i_{Ks} - \left(1/n_{Ks}\right)m_{Ks}^2. \quad (3)$$

In this study, a combination of stationary and nonstationary fluctuation methods was applied on experimental and simulated human recordings to identify the number n_{Ks} of I_{Ks} channels in the stochastic cell models. In brief, a value for the single channel current, i_{Ks}, was obtained from the experiments, and that value was taken as a reference to identify the number of I_{Ks} channels that, used in the stochastic simulations, led to a best match with the experimental i_{Ks} value. Specifically, experimental I_{Ks} current traces were measured in human ventricular myocytes after applying 5000-ms depolarizing voltage pulses from −40 mV to test potentials ranging from −10 to 50 mV (24). Because reliable I_{Ks} measurements could not be obtained immediately after the delivery of each pulse, but only ~100 ms after the transient change elicited by the pulse, ensemble mean and variance of the available I_{Ks} traces were computed at steady state for each of the test potentials. The nonstationary fluctuation analysis was used to estimate n_{Ks} and i_{Ks} by fitting the parabolic function of Eq. 3 to the variance-mean I_{Ks} data corresponding to the different test potentials (25). The mean channel open probability (p_{Ks}) was then computed as

$$p_{Ks} = \frac{m_{Ks}}{(i_{Ks}\ n_{Ks})}. \quad (4)$$

The mean channel open probability, p_{Ks}, was estimated at 50 mV (corresponding to the highest open probability). Some studies have reported that this method provides reliable estimates of p_{Ks}, but not of i_{Ks} or n_{Ks}, which cannot be robustly estimated unless some constraints on the variables to be estimated are imposed (26), particularly when voltages associated with low p_{Ks} are considered. Therefore, once an estimate of p_{Ks} was obtained at a specific voltage level (in this study, at 50 mV), a second method based on the stationary fluctuation analysis was used to estimate i_{Ks} (27). In this case, power spectral densities (PSDs) of mean-subtracted I_{Ks} current traces were computed, once I_{Ks} has reached steady state at the specific test potential. The unitary current i_{Ks} was estimated as the ratio between the integral of the averaged PSD divided by the product of 1-p_{Ks} and the time-averaged mean current (28).

Taking that experimental i_{Ks} estimate as a reference, fluctuation analysis was applied on simulated I_{Ks} current traces (obtained using the same voltage clamp protocol as in the experiments) and the best possible number of I_{Ks} channels in the stochastic human model was determined. In the simulations, reliable I_{Ks} measurements could be obtained from the beginning of the recordings, thus both the stationary and nonstationary methods could be applied on the simulated I_{Ks} traces at 50 mV. Results from the two methods were contrasted to ensure consistency of the identified n_{Ks} value.

For the guinea pig stochastic model, we considered the upper limit for the I_{Ks} unitary conductance estimated by Walsh et al. in experiments obtained with a filter cut-off frequency of 200 Hz (29). That value has been reported to be approximately half of the value found for human I_{Ks} currents expressed in *Xenopus* oocytes (28,30). We then used the frequency dependence data provided in (30) to extrapolate the unitary conductance value corresponding to 1 kHz, which is the cut-off frequency used in the human experiments, and we divided it by two to represent guinea pig myocytes. That process provided us with an estimate of 3.3 pS for the I_{Ks} unitary conductance in guinea pig, which we used to identify the corresponding number n_{Ks} of I_{Ks} channels in the model.

RESULTS AND DISCUSSION

Microscopic ion channel fluctuations modulate macroscopic ionic current kinetics

Intrinsic noise due to I_{Ks} stochastic gating was introduced in the model with parameters obtained from experimental traces using the approach described in the Materials and Methods section. In human, fluctuation analysis applied to experimental I_{Ks} data is presented in Fig. 1 *A*—variance-mean plots of steady I_{Ks} traces at different test potentials (*top third panel*), averaged I_{Ks} power spectral density at 50 mV (*top fourth panel*), and estimated single channel current (*bottom right panel*). As shown in Fig. 1 *A*, the single channel current estimated from experimental recordings of macroscopic I_{Ks} traces at 50 mV was $i_{Ks} = 0.762$ pA. This is in good agreement with previous values reported in the literature for currents formed by human KvLQT1 and minK subunits injected into *Xenopus* oocytes, where mean i_{Ks} was found to be 0.6 pA (28), and 0.8 pA (30). In guinea pig, I_{Ks} unitary conductance was estimated using available data from the literature (29,30), as described in the Methods section.

The i_{Ks}/unitary conductance values obtained from the experiments were then used to identify the number of I_{Ks} channels to be considered in the stochastic ventricular models, assuming that unitary current/conductance is uniform across cells (31). The number of I_{Ks} channels identified for the different simulated cell types was: in human, $n_{Ks} = 12{,}000$ for endocardial (endo) and epicardial (epi) cells and $n_{Ks} = 3000$ channels for midmyocardial (mid) cells; in guinea pig, $n_{Ks} = 20{,}000$ for epi, 6286 for endo, and 2286 for mid cells. To illustrate the time and frequency

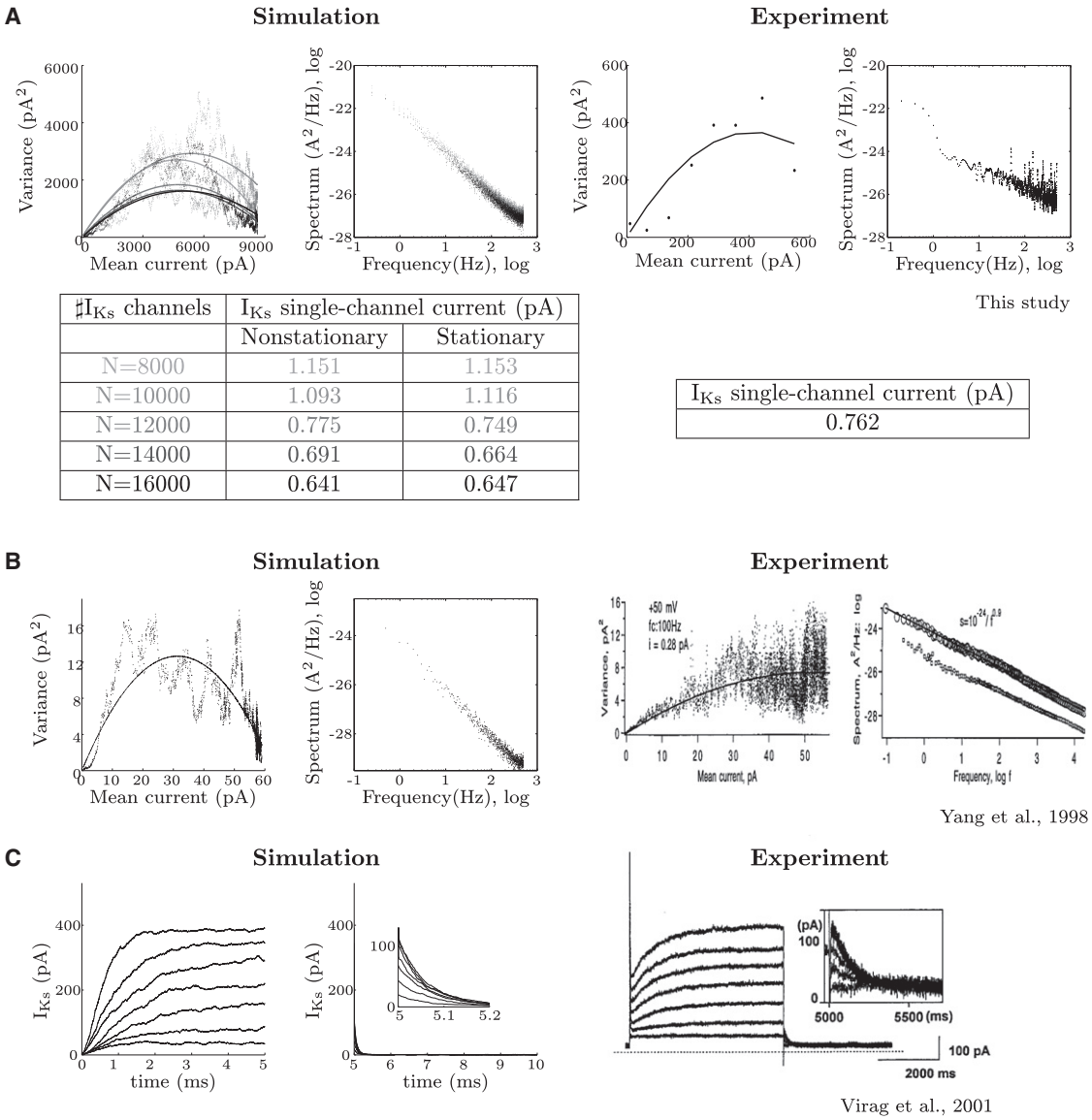

♯I_{Ks} channels	I_{Ks} single-channel current (pA)	
	Nonstationary	Stationary
N=8000	1.151	1.153
N=10000	1.093	1.116
N=12000	0.775	0.749
N=14000	0.691	0.664
N=16000	0.641	0.647

I_{Ks} single-channel current (pA)
0.762

FIGURE 1 Fluctuation analysis. (*A*) Nonstationary (variance-mean plots) and stationary (averaged PSDs) fluctuation analysis of simulated and experimental human I_{Ks} currents. Simulation results are computed from 20 sweeps for different numbers, n_{Ks}, of I_{Ks} channels: 8000, 10,000, 12,000, 14,000, and 16,000. Single channel current estimates are shown in each case. (*B*) Simulated and experimental (28) mean-variance plots and PSDs of human I_{Ks} currents at 50 mV. (*C*) Human I_{Ks} current traces, in simulations and experiments (24), following 5000-ms depolarizing voltage pulses from −40 mV to test potentials ranging from −10 to 50 mV in 10 mV-increments. In the simulations shown in *B* and *C*, n_{Ks} and the maximum I_{Ks} conductance, G_{Ks}, have been scaled down to match the maximum I_{Ks} amplitude of the experimental studies.

characteristics of simulated human I_{Ks} current fluctuations, Fig. 1 *A* presents variance-mean plots of I_{Ks} traces at 50 mV (*top first panel*), their averaged PSDs (*top second panel*), and estimated single channel currents (*bottom left panel*), for different channel numbers while keeping constant the maximum epicardial I_{Ks} conductance (G_{Ks}). That is, in all the simulations of Fig. 1 *A* G_{Ks} (= n_{Ks} i_{Ks} p_{Ks}) was kept at the constant value defined in the deterministic TP06 model, while in each case n_{Ks} was given a certain value (ranging from 8000 to 16,000) and i_{Ks} was correspondingly estimated from the fluctuation analysis applied to the simulated I_{Ks} traces).

Also shown in Fig. 1 is a comparison between our stochastic simulations and previous experimental studies of the literature (24,28), both in terms of fluctuation noise analysis (Fig. 1 *B*) and of I_{Ks} current traces (Fig. 1 *C*). Because I_{Ks} amplitude is very sensitive to the experimental cell isolation procedure (32) and presents wide variations across studies (24,28), n_{Ks} and G_{Ks} in the stochastic simulations of Fig. 1, *B* and *C*, were scaled to match the maximum I_{Ks} amplitude of the corresponding experimental set of data. Specifically, we assumed that during cell isolation the unitary conductance remains unaltered but a number of I_{Ks} channels are damaged. Therefore, we reduced n_{Ks} and G_{Ks}

by the same percentage in each case so that the maximum I_{Ks} amplitude in the simulations equaled the maximum I_{Ks} amplitude of the experimental set.

According to the results shown in Fig. 1, the time and frequency patterns of the simulated I_{Ks} currents are in good agreement with the experimental ones, indicating that our stochastic I_{Ks} model is able to reproduce intrinsic noise properties of experimental traces. Additional results on the contribution of ion channel fluctuations to macroscopic I_{Ks} variability are presented in the text and Fig. S1 of the Supporting Material, concluding that a large portion of the experimental cell-to-cell differences in I_{Ks} current properties can be explained by differences in I_{Ks} channel numbers (extrinsic noise) rather than by I_{Ks} random gating (intrinsic noise). Results shown later in the study were obtained with the n_{Ks} values derived from the fluctuation analysis with no subsequent scaling, which was only applied when comparing simulated and experimental I_{Ks} current values (i.e., in Fig. 1, *B* and *C*, and Fig. S1).

Channel numbers determine temporal and spatial electrophysiological heterogeneity

The impact of I_{Ks} fluctuations on temporal cell variability was investigated by using the developed and validated stochastic cell models and the previously identified channel numbers. Fig. S2 shows examples of beat-to-beat variability in action potential duration (APD) in isolated guinea pig (Fig. S2 *A*) and human (Fig. S2 *B*) ventricular myocytes. APs were obtained for 20 consecutive cardiac cycles from simulations and experiments at 1 Hz steady-state pacing (0.5 Hz for the study by Zaniboni et al. (7)). In simulated guinea pig myocytes, averaged temporal APD ranges (computed from a set of 15 independent stochastic realizations) were 6/10/4 ms for endo/mid/epi cells. In the guinea pig experiments of this study shown in Fig. S2 *A*, APD ranges were 10, 10, 14, and 12 ms for representative apical-epi, apical-endo, basal-epi, and basal-endo cells, respectively, and in the experiment of Zaniboni et al. (7) the APD range was 25 ms. In human, simulated APD ranges were 10/15/10 ms for endo/mid/epi cells, whereas in the experiment of this study the range was 18 ms. Additionally, canine experiments were performed in this study, where the averaged range of APD temporal variability was 13 ms. A major conclusion is the confirmation that differences in I_{Ks} channel numbers determine temporal variability in the AP in the three cell layers. In both species, the lower number of I_{Ks} channels in mid cells, as compared to endo and epi cells, translated into larger beat-to-beat variability in APD, with variability being larger in human than in guinea pig—see the Supporting Material for further results and discussion. In all cases, AP temporal variability in the simulations was in the experimentally observed range.

Next, cell-to-cell variability was investigated by additionally introducing extrinsic noise in the simulations, with the number of I_{Ks} channels for each simulated cell extracted from a truncated Gaussian distribution with mean equal to the n_{Ks} value provided previously. Simulated cell-to-cell APD variability in guinea pig and human is shown in Fig. 2, and compared with experiments performed in isolated ventricular myocytes. In the left part of Fig. 2 *A* and in Fig. 2 *B*, simulated guinea pig and human APs associated with minimum and maximum APD values over 15 stochastic realizations, corresponding to 15 different simulated myocytes, are presented. Results are grouped according to layer in the ventricular wall, and correspond to the same simulated beat under steady-state pacing at 1 Hz. Large differences were observed in the APDs of two distinct myocytes, even when simulated from the same ventricular layer, with maximal differences of 32/30/74 ms for simulated endo/mid/epi guinea pig cells and 176/109/130 ms for human. The simulated guinea pig values were within the experimental APD differences measured in this study for myocytes isolated from the same location and heart, as shown by the representative examples in the right part of Fig. 2 *A*. Notably larger experimental differences were observed when comparing myocytes from the same location but different hearts. A summary of guinea pig and human cell-to-cell APD differences in simulations and experiments is presented in the bar charts of Fig. S3, with simulated differences always lying within experimental ranges (33,34).

Cellular coupling mitigates manifestation of ion channel fluctuations in ventricles

The impact of ion channel fluctuations was evaluated when cells were coupled in a transmural 1D fiber and in an anatomically based ventricular geometry, with both intrinsic and extrinsic noises included in the I_{Ks} current formulation. The effect of coupling on temporal variability was first assessed. Simulated beat-to-beat APD variability is presented in Fig. 3 *A* (*left panel*), for an electrically coupled guinea pig mid cell of the transmural fiber and an isolated mid cell. Electrotonic coupling results in a 90% reduction in the APD range over 20 consecutive cardiac cycles at 1 Hz pacing. Simulations using the whole ventricular geometry confirmed the results obtained from the 1D cable. In endo and epi guinea pig cells, percentages of reduction were 83% and 75%, respectively. In the experiments of Zaniboni et al. (7), coupling reduced the APD range by 51% (Fig. 3 *A*, *right panel*). In our human simulations, coupling reduced the APD range in epi, endo, and mid cells by 80%, 80%, and 87%, consistent with a 72% reduction in human experimental data (Fig. 3 *B*). In dog experiments, the averaged APD range decreased by 69%. Further results on mitigation of temporal variability due to the effect of coupling are presented in the Supporting Material (expressed in relative terms as coefficient of variation).

The effect of coupling on modulating spatial variability was also investigated. Cell-to-cell APD differences between

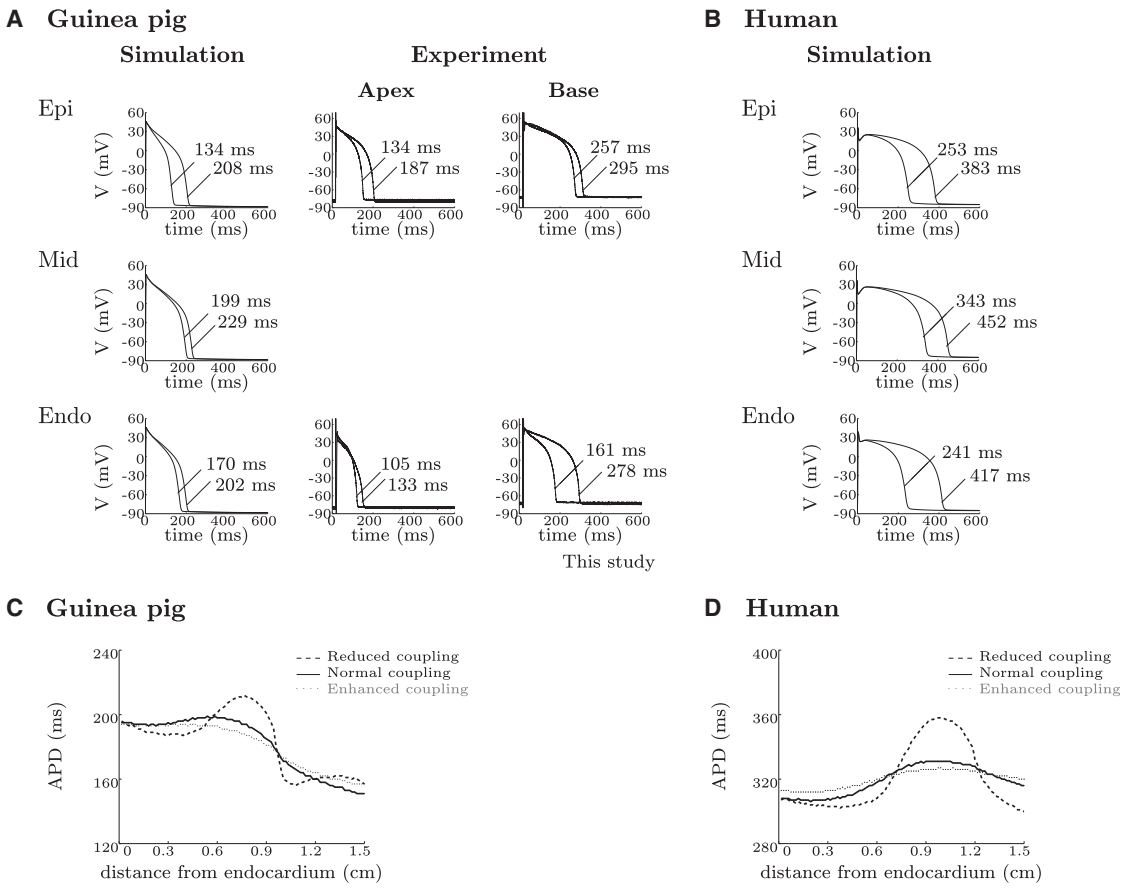

FIGURE 2 Spatial APD variability. (*A*) Simulated and experimental APs of guinea pig myocytes at 1 Hz pacing, corresponding to minimum and maximum APD across cells ($n = 15$ for simulations, and $n = 2, 2, 2$ and 4 for experiments). (*B*) Analogous results in human ($n = 15$ for simulations). (*C* and *D*): APD profiles in simulated guinea pig and human 1D fibers, computed at 1 Hz steady state for three degrees of coupling (reduced, normal, and enhanced).

the coupled myocytes of the simulated transmural fiber are shown in Fig. 2 for guinea pig (*panel C*) and human (*panel D*). APD profiles are presented for three different degrees of coupling representing reduced, normal, and enhanced electrical coupling. The diffusion coefficient for each case was 0.165 (0.234), 0.826 (1.171), and 1.487 (2.108) cm^2/s in guinea pig (human), respectively, and averaged conduction velocities at 1 Hz steady-state pacing were 14.9 (22.7), 45.5 (60.0), and 62.5 (83.3) cm/s in guinea pig (human), respectively. As illustrated in Fig. 2, coupling acted to decrease spatial APD variability across the wall and within each of the three layers. Specifically, maximal APD differences within the mid layer of the guinea pig (respectively human) 1D fiber were 28 (22), 23 (5), and 19 (3) ms under reduced, normal, and enhanced coupling, respectively, as compared with 30 (109) ms found for isolated mid myocytes. Those tissue APD differences obtained with the stochastic model in the mid layer were relatively close, ± 6 (± 2) ms, to those found for the deterministic model. The maximum transmural difference in APD in the stochastic simulations was of 45 (25) ms for guinea pig (human) under normal coupling, and it increased by 27 (144)% and decreased by 11 (36)% under reduced and enhanced coupling, respectively. In both guinea pig and human, transmural APD differences obtained with the stochastic model were only slightly different (± 2 ms) from those found with the deterministic model. All the previous results show that, in tissue, intercellular coupling acts to suppress the important role of I_{Ks} stochasticity in modulating beat-to-beat and cell-to-cell variability in APD observed in isolated cardiomyocytes.

Finally, the manifestation of I_{Ks} stochasticity was investigated in pseudo-ECGs (see text and Fig. S4 in the Supporting Material). Temporal variability in the pseudo-ECG is shown to be of very low magnitude under control conditions, but reduced coupling acted to slightly unmask temporal fluctuations in the pseudo-ECG.

Pathology accentuates the proarrhythmic consequences of ion channel fluctuations

In this study, we hypothesize that pathological conditions affecting repolarization reserve might potentiate the role of stochastic I_{Ks} gating in modulating variability in APD. Our simulations show that I_{Kr} block increased temporal APD variability in guinea pig and human. In both cases, the increase was more prominent in mid cells than in endo

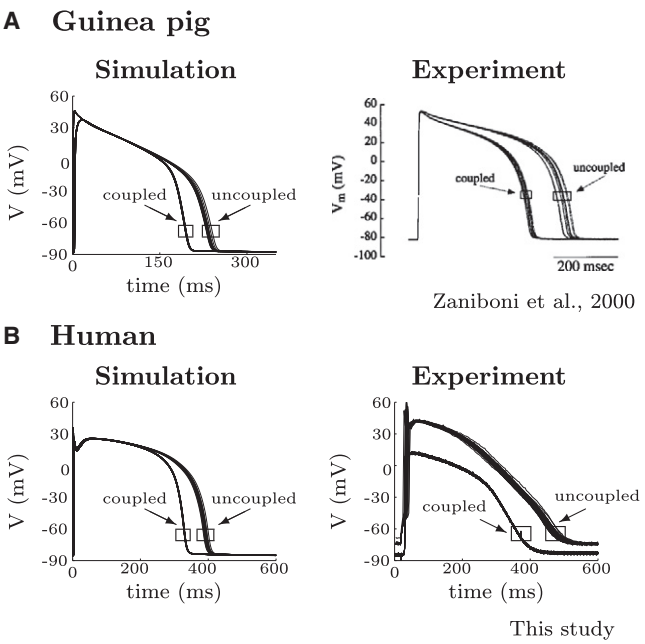

FIGURE 3 Temporal variability in uncoupled and coupled mid myocytes from simulations and experiments (measured in this study and reproduced from (7)) for guinea pig (*A*) and human (*B*).

and epi cells due to differences in channel numbers (>8000% increase in guinea pig due to abnormal depolarizations interrupting AP repolarization and 92% increase in human in mid cells, as compared to >8000% and 30%, respectively, in endo and 25% and 20%, respectively, in epi cells). Elevated temporal variability due to I_{Kr} block was also observed for cells coupled into tissue with elevated variability being also more prominent in the midmyocardial region due to its associated lower number of I_{Ks} channels (188%, 213%, and 61% increase in APD range for cells in the central part of endo, mid, and epi regions within the simulated guinea pig 1D fiber, and 8%, 27%, and 23% for the human 1D fiber). Our results are consistent with observations from experimental studies reported in the literature (7,35,36) and with the experiment on a human myocyte conducted in this study, where the APD range was increased by 278% after blocking I_{Kr}. In addition, the canine experiments of this study confirmed our observation that the increase in the APD range after dofetilide injection (full I_{Kr} block) was more prominent in single cells than in tissue, with averaged increases of 370% and 39%, respectively.

I_{Kr} block also accentuated cell-to-cell APD differences in isolated myocytes and spatial APD dispersion in tissue. In the 1D tissue simulations, transmural APD differences at normal coupling were of 174 and 34 ms under full I_{Kr} block in guinea pig and human, respectively, which represent around 4 and 1.5 times the APD variability values found in control.

Under I_{Kr} block, there were increases in the temporal ranges of the QT interval of 526% in guinea pig and 43% in human (see the Supporting Material). Nevertheless, the variability levels observed after blocking I_{Kr} were only of some relevance when measured in single cells, but not in tissue or ECG at physiological coupling due to the effect of electrotonic interactions working to synchronize APDs of neighboring cells (7). Simulation of reduced coupling conditions, as documented in diseased hearts, confirmed the role of temporal repolarization variability in facilitating the occurrence of electrical instabilities, as seen by complex patterns of APD and QT Poincaré plots, in accord with experimental and clinical data (1,2,37) (see Fig. S4 and text in the Supporting Material).

Of importance, our simulations show that I_{Ks} stochastic fluctuations in the presence of I_{Kr} block favored the appearance of repolarization abnormalities such as early afterdepolarization (EAD) formation (2,3). EAD occurrence was promoted by a sudden change in the stimulation frequency from 1 to 0.4 Hz (Fig. 4). In guinea pig cells, I_{Kr} blockade in the deterministic model only resulted in EADs in mid cells, while with stochastic I_{Ks}, EADs occurred in 21/95/16% of endo/mid/epi cells. In human, EADs was not observed in the deterministic model for any cell type under I_{Kr} block. However, the consideration of I_{Ks} fluctuations in the model led to EADs in 20% of the simulations for mid cells. The ability of I_{Kr} block to produce EADs, more so in mid cells than in endo or epi cells, reported from the stochastic simulations of this study is in agreement with findings from experiments conducted in different species, including guinea pig and human (35,38–40) and also with the canine experiments of this study, where EADs developed in 50% (2 out of 4) of the analyzed cells after dofetilide injection—Fig. 5 *A*.

Coupling acted to modulate the likelihood of EAD occurrence in tissue following rate deceleration. In the presence of I_{Ks} stochasticity, EADs were observed after full I_{Kr} block in one-fifth of the guinea pig 1D tissue containing endo and mid cells, but were not observed when simulating the whole ventricular geometry. When coupling was moderately decreased by 30%, the 1D tissue portion presenting EADs was enlarged, occupying one-third of the tissue (endo-mid region). In human tissue, EADs was not seen in any simulation, consistent with the results of the canine experiments of this study, where EADs was not induced in tissue exposed to dofetilide (Fig. 5 *B*). Furthermore, nor even after simulating 80% coupling reduction could EADs be observed in human tissues. Our results show that I_{Ks} stochasticity enhances the probability of EAD formation, whereas electrotonic flow due to intercellular coupling counteracts this effect. This could have major implications for the genesis of arrhythmias as it suggests that under normal coupling it is difficult for those EADs to develop and propagate, even if I_{Kr} is fully blocked. However, abnormal conditions involving reduced levels of cell-to-cell coupling, as in heart failure or myocardial ischemia, could render the myocardium more vulnerable to the occurrence of EADs following I_{Kr} block,

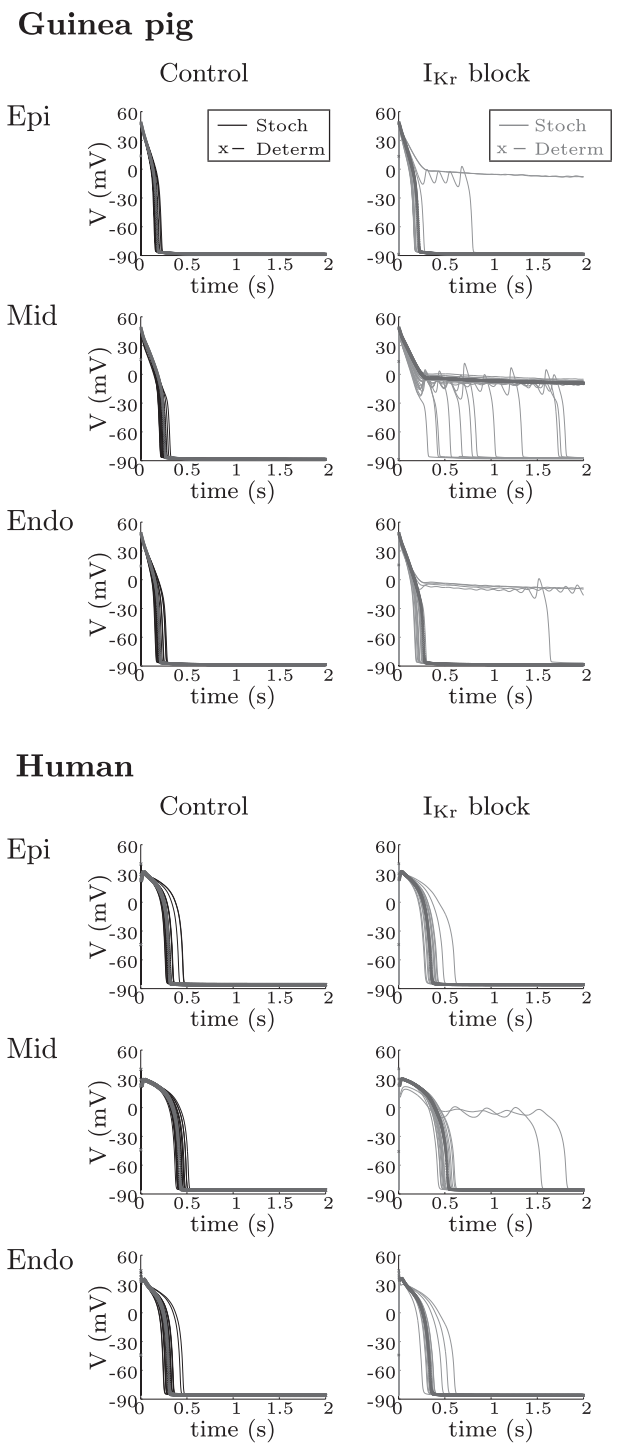

FIGURE 4 EAD generation. (*A*) Simulated APs obtained after suddenly changing pacing rate from 1 to 0.4 Hz using the deterministic FR07 guinea pig model (*black dashed* for control, and *gray dashed* for I_{Kr} block) and 20 different realizations of the stochastic guinea pig model (*black solid* for control, and *gray solid* for I_{Kr} block). (*B*) Analogous results for human.

which could in turn trigger arrhythmias if they occurred in a substantial mass of the ventricle.

Increased temporal variability due to I_{Ks} fluctuations also facilitates the occurrence of APD alternans. APD alternans, defined as alternations in the APD of the form long-short-long-short, occur at rapid rates of stimulation and have been shown to be predictive of arrhythmia development (5). In this study, the threshold frequency for APD alternans was determined as the lowest frequency for which differences in APD values of at least eight consecutive beats were >10 ms (41). That threshold was found to be lowered when stochastic I_{Ks} fluctuations were introduced into the deterministic models; particularly under I_{Kr} block conditions (see text and Fig. S5 in the Supporting Material).

Repolarization alternans were not observed in physiologically coupled tissue (transmural 1D fiber or whole ventricular geometry) at any stimulation frequency either under control or full I_{Kr} block, but were observed in the mid layer at reduced coupling. The thresholds for APD alternans in tissue were of 8.3 and 3.3 Hz in guinea pig and human under control, and 5.7 and 2.9 Hz under I_{Kr} block, in both cases after 80% coupling reduction. These results on the increased likelihood of APD alternans (as an extreme form of beat-to-beat variability) in diseased hearts presenting reduced levels of electrotonic coupling are in agreement with experimental data (42).

Study limitations and future research

This combined experimental and theoretical study provides an in-depth characterization of the role played by intrinsic and extrinsic noise due to I_{Ks} channel gating and cell-to-cell differences in I_{Ks} density in determining variability in cardiac repolarization. The following points include a number of questions arising from the current study that remain to be addressed through further research:

1. Cell and tissue AP models were developed where the I_{Ks} current was modeled as a stochastic process but all of the other model components were deterministic. The I_{Ks} characteristics of slow kinetics and small associated number of channels suggest an important contribution to repolarization variability (9). However, modeling intrinsic and extrinsic noises in other transmembrane ionic currents and calcium dynamics would allow identifying the most relevant causes of APD variability. This was attempted in recent computational studies (see, for instance (13,16)), and experimental confirmation is required.
2. Attention was focused on variability that originates under constant pacing rates and autonomic influences were not at all considered. Future studies should investigate the effects of I_{Ks} stochasticity on cell and tissue variability in situations involving high levels of β-adrenergic stimulation, where the role of I_{Ks} has been suggested to be more relevant (8).
3. Other electrophysiological sources not modeled in this study may additionally contribute to repolarization variability, including differences in cell geometry or

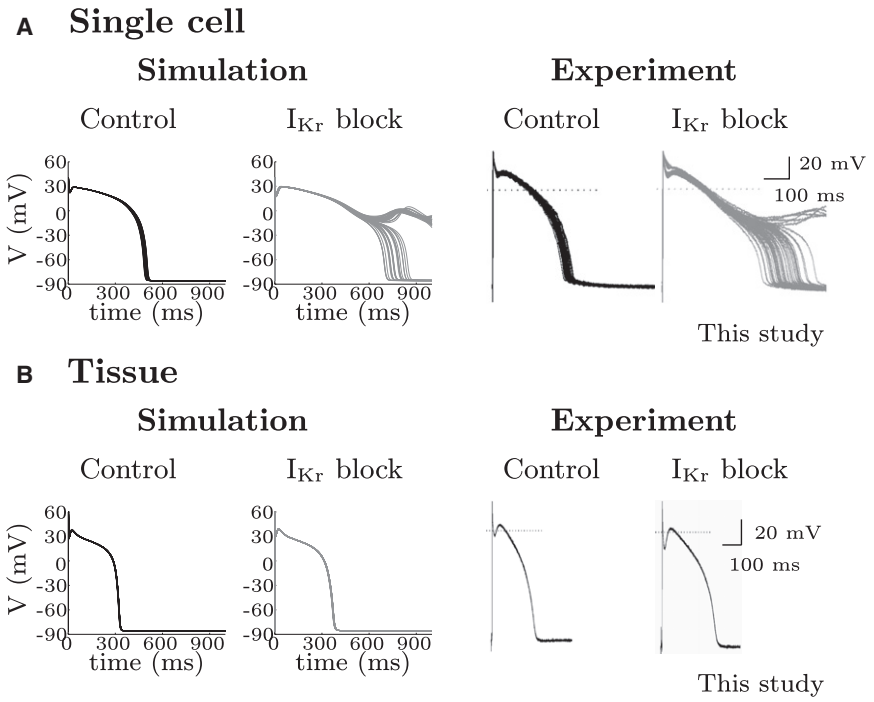

FIGURE 5 Temporal variability and presence/absence of EADs in single cell (*A*) and tissue (*B*) from human simulations and canine experiments under control (*black line*) and following I_{Kr} block (*gray line*).

tissue structure, and heterogeneities in electrotonic coupling (37).

4. The I_{Ks} current in the deterministic TP06 human ventricular model, taken as the basis for our stochastic human model, is much larger than in experimental studies (24,28) and other human ventricular cell models recently published (43,44). Because I_{Ks} density is large in the model, there are an associated high number of I_{Ks} channels, and, as a consequence, the effects of channel gating on cell and tissue variability are attenuated. The results of our study in human myocytes could be interpreted as providing a lower limit for the effects of I_{Ks} stochasticity on repolarization variability and associated arrhythmogenic implications.
5. The bandwidth of the experimental recordings has a notable influence in the fluctuation analysis. If the bandwidth is not sufficient, the variance of the current fluctuations is underestimated, which correspondingly leads to underestimates of unitary current. This in turn implies a larger number of I_{Ks} channels in the model, and reduced variability at all levels. Experimental studies using data sampled at frequencies varying from 0.25 to 25 kHz have shown that below 10 kHz the conductance values obtained from fluctuation analysis are affected by a lack of convergence of the current variance. In this study, experimental I_{Ks} current traces recorded in human myocytes were filtered at 1 kHz. Based on this, we acknowledge a limitation for a more accurate evaluation of I_{Ks} channel noise. An illustration of the potential effects that larger I_{Ks} noise levels, accounting for higher frequency components in experimental I_{Ks} traces, may have on APD variability and arrhythmogenesis is presented in Fig. S6, showing results obtained by decreasing n_{Ks} while keeping G_{Ks} constant. Despite the acknowledged limitation, the unitary current of I_{Ks} channels estimated in this study was 0.762 pA, which is very similar to the 0.6 ± 0.2 pA found by Yang et al. (28), and 0.8 ± 0.2 pA found by Sesti et al. (30) for human I_{Ks} currents expressed in *Xenopus* oocytes, which were exclusively used in this study for comparison purposes. In terms of I_{Ks} unitary conductance, the estimated value from our experiments was 5.8 pS, which is comparable to the 6.6 pS found in (30) for a corresponding cut-off frequency of 1 kHz. Future studies should evaluate the impact of the filter cut-off frequency on the estimation of single channel current/unitary conductance of membrane ionic currents from intact human myocytes.

CONCLUSIONS

In this study, a combined experimental and computational multiscale investigation is conducted to unravel the role played by I_{Ks} stochasticity in modulating beat-to-beat and cell-to-cell variability in ventricular repolarization. To the best of our knowledge, this is the first study where careful construction and validation of mathematical models of I_{Ks} stochasticity is performed to guarantee reliable conclusions on its role in determining ventricular repolarization variability in health and disease. The results suggest that stochastic I_{Ks} gating and channel numbers are important contributors to temporal and spatial variability in isolated

cells, but their effects are masked in tissue due to electrotonic interactions. Pathological conditions resulting in reduced repolarization reserve (e.g., I_{Kr} block) or in intercellular uncoupling (e.g., acidosis) could uncover the manifestation of stochastic I_{Ks} properties resulting in enhanced variability and proarrhythmic abnormalities in repolarization such as afterdepolarizations and alternans.

SUPPORTING MATERIAL

Further details and results, references, and six figures are available at http://www.biophysj.org/biophysj/supplemental/S0006-3495(11)01241-0.

The authors are grateful to Christian Bollensdorff and Peter Kohl for their contribution to the guinea pig experiments. The authors thank the reviewers for their valuable comments.

This study was supported by the European Commission preDiCT grant (DG-INFSO-224381), UK Medical Research Council Career Development Award (B.R.), Royal Society International Joint Project (E.P., B.R.), grant TEC2010-19410 from Ministerio de Ciencia e Innovación, PI 144/2009 and T30 from Gobierno de Aragón, Spain (E.P.), and grants OTKA CNK-77855 from Hungarian Scientific Research Fund, TECH_08_A1_CARDIO08 from National Office Research and Technology–Ányos Jedlik Programme, and TÁMOP-4.2.2-08/1-2008-0013 and TÁMOP-4.2.1/B-09/1/KONV-2010-0005 National Development Agency cofinanced by the European Regional Fund, Hungary (L.V., N.J., T.S., A.V., N.S., P.P.N.).

REFERENCES

1. Hondeghem, L. M., L. Carlsson, and G. Duker. 2001. Instability and triangulation of the action potential predict serious proarrhythmia, but action potential duration prolongation is antiarrhythmic. *Circulation.* 103:2004–2013.
2. Thomsen, M. B., S. C. Verduyn, …, M. A. Vos. 2004. Increased short-term variability of repolarization predicts d-sotalol-induced torsades de pointes in dogs. *Circulation.* 110:2453–2459.
3. Johnson, D. M., J. Heijman, …, P. G. Volders. 2010. *I*(Ks) restricts excessive beat-to-beat variability of repolarization during beta-adrenergic receptor stimulation. *J. Mol. Cell. Cardiol.* 48:122–130.
4. Hinterseer, M., B. M. Beckmann, …, S. Kääb. 2010. Usefulness of short-term variability of QT intervals as a predictor for electrical remodeling and proarrhythmia in patients with nonischemic heart failure. *Am. J. Cardiol.* 106:216–220.
5. Myles, R. C., F. L. Burton, …, G. L. Smith. 2008. The link between repolarization alternans and ventricular arrhythmia: does the cellular phenomenon extend to the clinical problem? *J. Mol. Cell. Cardiol.* 45:1–10.
6. Lerma, C., T. Krogh-Madsen, …, L. Glass. 2007. Stochastic aspects of cardiac arrhythmias. *J. Stat. Phys.* 128:347–374.
7. Zaniboni, M., A. E. Pollard, …, K. W. Spitzer. 2000. Beat-to-beat repolarization variability in ventricular myocytes and its suppression by electrical coupling. *Am. J. Physiol. Heart Circ. Physiol.* 278:H677–H687.
8. Severi, S., C. Corsi, …, A. Zaza. 2009. Mechanisms of beta-adrenergic modulation of *I*(Ks) in the guinea-pig ventricle: insights from experimental and model-based analysis. *Biophys. J.* 96:3862–3872.
9. Krogh-Madsen, T. 2004 Effects of single-channel noise on spontaneous beating and the phase-resetting response of cardiac oscillators. PhD thesis. McGill University, Montreal, Canada.
10. Fox, R. F. 1997. Stochastic versions of the Hodgkin-Huxley equations. *Biophys. J.* 72:2068–2074.
11. Mino, H. J., J. T. Rubinstein, and J. A. White. 2002. Comparison of algorithms for the simulation of action potentials with stochastic sodium channels. *Ann. Biomed. Eng.* 30:578–587.
12. Ponard, J. G., A. A. Kondratyev, and J. P. Kucera. 2007. Mechanisms of intrinsic beating variability in cardiac cell cultures and model pacemaker networks. *Biophys. J.* 92:3734–3752.
13. Tanskanen, A. J., J. L. Greenstein, …, R. L. Winslow. 2005. The role of stochastic and modal gating of cardiac L-type Ca^{2+} channels on early after-depolarizations. *Biophys. J.* 88:85–95.
14. Sato, D., L. H. Xie, …, Z. Qu. 2009. Synchronization of chaotic early afterdepolarizations in the genesis of cardiac arrhythmias. *Proc. Natl. Acad. Sci. USA.* 106:2983–2988.
15. Silva, J. R., H. Pan, …, Y. Rudy. 2009. A multiscale model linking ion-channel molecular dynamics and electrostatics to the cardiac action potential. *Proc. Natl. Acad. Sci. USA.* 106:11102–11106.
16. Lemay, M., E. de Lange, and J. P. Kucera. 2011. Effects of stochastic channel gating and distribution on the cardiac action potential. *J. Theor. Biol.* 281:84–96.
17. Pueyo, E., A. Corrias, D. Gavaghan, K. Burrage, and B. Rodríguez. 2009. Role of I_{Ks} gating kinetics in arrhythmogenesis. *Heart Rhythm,* Supplement, Abstract, S296.
18. ten Tusscher, K. H., and A. V. Panfilov. 2006. Alternans and spiral breakup in a human ventricular tissue model. *Am. J. Physiol. Heart Circ. Physiol.* 291:H1088–H1100.
19. Faber, G. M., J. Silva, …, Y. Rudy. 2007. Kinetic properties of the cardiac L-type Ca^{2+} channel and its role in myocyte electrophysiology: a theoretical investigation. *Biophys. J.* 92:1522–1543.
20. Van Kampen, N. G. 1992. Stochastic Processes in Physics and Chemistry. North–Holland, Amsterdam.
21. Gima, K., and Y. Rudy. 2002. Ionic current basis of electrocardiographic waveforms: a model study. *Circ. Res.* 90:889–896.
22. Corrias, A., X. Jie, …, B. Rodriguez. 2010. Arrhythmic risk biomarkers for the assessment of drug cardiotoxicity: from experiments to computer simulations. *Philos. Transact. A Math. Phys. Eng. Sci.* 368: 3001–3025.
23. Hille, B. 2001. Ion Channels of Excitable Membranes. Sinaure Associates, Sunderland, MA.
24. Virág, L., N. Iost, …, J. G. Papp. 2001. The slow component of the delayed rectifier potassium current in undiseased human ventricular myocytes. *Cardiovasc. Res.* 49:790–797.
25. Sigworth, F. J. 1980. The variance of sodium current fluctuations at the node of Ranvier. *J. Physiol.* 307:97–129.
26. Lingle, C. J. 2006. Empirical considerations regarding the use of ensemble-variance analysis of macroscopic currents. *J. Neurosci. Methods.* 158:121–132.
27. Sigworth, F. J. 1981. Interpreting power spectra from nonstationary membrane current fluctuations. *Biophys. J.* 35:289–300.
28. Yang, Y., and F. J. Sigworth. 1998. Single-channel properties of I_{Ks} potassium channels. *J. Gen. Physiol.* 112:665–678.
29. Walsh, K. B., J. P. Arena, …, R. S. Kass. 1991. Delayed-rectifier potassium channel activity in isolated membrane patches of guinea pig ventricular myocytes. *Am. J. Physiol.* 260:H1390–H1393.
30. Sesti, F., and S. A. Goldstein. 1998. Single-channel characteristics of wild-type I_{Ks} channels and channels formed with two minK mutants that cause long QT syndrome. *J. Gen. Physiol.* 112:651–663.
31. Furukawa, T., S. Kimura, …, R. J. Myerburg. 1992. Potassium rectifier currents differ in myocytes of endocardial and epicardial origin. *Circ. Res.* 70:91–103.
32. Yue, L., J. Feng, …, S. Nattel. 1996. Transient outward and delayed rectifier currents in canine atrium: properties and role of isolation methods. *Am. J. Physiol.* 270:H2157–H2168.
33. Bryant, S. M., X. Wan, …, G. Hart. 1998. Regional differences in the delayed rectifier current (I_{Kr} and I_{Ks}) contribute to the differences in action potential duration in basal left ventricular myocytes in guinea-pig. *Cardiovasc. Res.* 40:322–331.

34. Li, G. R., J. Feng, …, M. Carrier. 1998. Transmural heterogeneity of action potentials and Ito1 in myocytes isolated from the human right ventricle. *Am. J. Physiol.* 275:H369–H377.

35. Sicouri, S., M. Quist, and C. Antzelevitch. 1996. Evidence for the presence of M cells in the guinea pig ventricle. *J. Cardiovasc. Electrophysiol.* 7:503–511.

36. Bargheer, K., F. Bode, …, P. R. Lichtlen. 1994. Prolongation of monophasic action potential duration and the refractory period in the human heart by tedisamil, a new potassium-blocking agent. *Eur. Heart J.* 15:1409–1414.

37. Poelzing, S., and D. S. Rosenbaum. 2004. Nature, significance, and mechanisms of electrical heterogeneities in ventricle. *Anat. Rec. A Discov. Mol. Cell. Evol. Biol.* 280:1010–1017.

38. Spitzer, K. W., A. E. Pollard, …, D. J. Huelsing. 2006. Cell-to-cell electrical interactions during early and late repolarization. *J. Cardiovasc. Electrophysiol.* 17 (*Suppl 1*):S8–S14.

39. Veldkamp, M. W., A. O. Verkerk, …, T. Opthof. 2001. Norepinephrine induces action potential prolongation and early afterdepolarizations in ventricular myocytes isolated from human end-stage failing hearts. *Eur. Heart J.* 22:955–963.

40. Burashnikov, A., and C. Antzelevitch. 2002. Prominent *I*(Ks) in epicardium and endocardium contributes to development of transmural dispersion of repolarization but protects against development of early afterdepolarizations. *J. Cardiovasc. Electrophysiol.* 13:172–177.

41. Wan, X., K. R. Laurita, …, D. S. Rosenbaum. 2005. Molecular correlates of repolarization alternans in cardiac myocytes. *J. Mol. Cell. Cardiol.* 39:419–428.

42. Kjølbye, A. L., M. Dikshteyn, …, D. S. Rosenbaum. 2008. Maintenance of intercellular coupling by the antiarrhythmic peptide rotigaptide suppresses arrhythmogenic discordant alternans. *Am. J. Physiol. Heart Circ. Physiol.* 294:H41–H49.

43. Grandi, E., F. S. Pasqualini, and D. M. Bers. 2010. A novel computational model of the human ventricular action potential and Ca transient. *J. Mol. Cell. Cardiol.* 48:112–121.

44. O'Hara, T., L. Virág, …, Y. Rudy. 2011. Simulation of the undiseased human cardiac ventricular action potential: model formulation and experimental validation. *PLOS Comput. Biol.* 7:e1002061.

A Multiscale Investigation of Repolarization Variability and Its Role in Cardiac Arrhythmogenesis

Esther Pueyo,[†‡§] Alberto Corrias,[†] László Virág,[¶] Norbert Jost,[‖] Tamás Szél,[¶] András Varró,[¶‖] Norbert Szentandrássy,[**] Péter P. Nánási,[**] Kevin Burrage,[†] and Blanca Rodríguez[†]

[†]Computing Laboratory, University of Oxford, Oxford, United Kingdom; [‡]Aragón Institute of Engineering Research, IIS Aragón, Universidad de Zaragoza, Zaragoza, Spain; [§]Biomedical Research Networking Center in Bioengineering, Biomaterials and Nanomedicine, Zaragoza, Spain; [¶]Department of Pharmacology and Pharmacotherapy, University of Szeged, Szeged, Hungary; [‖]Division of Cardiovascular Pharmacology, Hungarian Academy of Sciences, Szeged, Hungary; and [**]Department of Physiology, University of Debrecen, Debrecen, Hungary

Supporting Material

Supporting Material Text

Stochastic cellular AP models

Cell-to-cell differences in the number of I_{Ks} channels, n_{Ks}, were modeled by including extrinsic noise following a truncated Gaussian distribution. The mean m_n was taken as the estimated n_{Ks} value derived from the fluctuation analysis, while the standard deviation σ_n was computed as one half of m_n to match the dispersion values obtained from experimental I_{Ks} current data available for this study as well as from the literature (1-4). The bounds for n_{Ks} in the truncation of the Gaussian distribution were defined to guarantee plausible AP durations from the simulations. The range of AP durations, computed for both human and guinea pig, were defined based on available experimental data (3,5-12), independent of the set of data used for model validation purposes.

Transmural heterogeneities in the densities of I_{Ks} and I_{to} were introduced in the stochastic AP models developed in this work following the approaches used in previous studies (13,14). Specifically, in human, the maximum conductance G_{Ks} of I_{Ks} was set to 0.392 nS/pF for endo and epi cells, and 0.098 nS/pF for mid cells. The maximum conductance G_{to} of I_{to} was set to 0.073 nS/pF for endo, and 0.294 nS/pF for mid and epi cells. In guinea pig, G_{Ks} was defined as a function of the intracellular calcium concentration, Ca_i, being $G_{Ks} = (0.433)\cdot(1+0.6/(1+ (0.000038/Ca_i)^{1.4}))$ for epi cells, and 0.3143 and 0.1143 times that value for endo and mid cells, respectively. G_{to} was defined as 0 (not expressed), 0.425, and 0.5 nS/pF for endo, mid, and epi cells, respectively. Since G_{Ks} is directly proportional to the number of I_{Ks} channels, n_{Ks} was scaled accordingly in the SDEs that define the I_{Ks} gating variables.

Tissue models

A monodomain reaction-diffusion equation was used to model the propagation of the cellular APs across the cardiac tissue:

$$\nabla\left(\frac{D}{C}\right)\cdot\nabla V = \frac{\partial V}{\partial t} + \frac{I_{ion}}{C} \qquad (1)$$

where D is the diffusion coefficient in the ventricular tissue, C is the membrane capacitance (set to 153 pF for guinea pig, and 185 pF for human), and I_{ion} represents the sum of the externally applied current and all the transmembrane ionic currents computed using the stochastic cell models of this study. Tissue simulations were conducted using a transmural 1D fiber consisting of 100 guinea pig (analogously, human) cells, as well as an anatomically-based rabbit ventricular mesh composed of 431990 tetrahedral elements (15) used for guinea pig simulations only. For the 1D fiber simulations, the normalized diffusion coefficient, D/C, was set to a constant value of 0.826 cm^2/s in guinea pig (14), and 1.171 cm^2/s in human (16), except for a 5-fold decrease at the transition between mid and epi regions (14), and no-flux boundary conditions were imposed. For the whole ventricle simulations, the normalized diffusion coefficient was 0.43 cm^2/s. Transmural layers were divided in relative proportions of 4:3:4 for endo, mid and epi layers in guinea pig (14) and 5:3:2 in human (16). In order to approximate ventricular activation by the Purkinje system, an intracellular stimulus was applied to the endocardial end of the fiber in the 1D simulations, and to cells belonging to the endocardial surface and located in the apical 27% of the heart for the whole ventricle simulations.

The ODEs defining the state variables of the AP models were solved using the Forward Euler method with a time step of 0.02 ms. A step size of this value is known to produce stable behavior in the numerics. The SDE defined in this study for the stochastic human model and analogous SDEs for the guinea pig model were integrated using the Euler Maruyama method

also with a time step of 0.02 ms. The partial differential equation (PDE) of Eq. 1 was solved using second-order central differences with a space step of 0.015 cm and a time step of 0.02 ms in the case of the fiber simulations, whereas in the whole ventricle simulations it was solved using a standard Galerkin finite element method with linear basis functions and a time step of 0.01 ms by means of the Chaste software package (17).

ECG calculation

The extracellular unipolar potential or pseudo-ECG (p) at a location (x_0, y_0, z_0) was calculated using the following expression:

$$p(x_0, y_0, z_0) = -\int_{\Omega} \beta \nabla V \cdot \nabla \frac{1}{r} dv \quad (2)$$

where β is the diffusion coefficient of the electrical medium surrounding the heart, Ω denotes the ventricular tissue length or volume, r is the distance between the recording electrode (x_0, y_0, z_0) and a point (x, y, z) within the ventricular tissue, $r = [(x-x_0)^2+(y-y_0)^2+(z-z_0)^2]^{1/2}$, and dv is the spatial resolution of the tissue. For the 1D simulations, the electrode was assumed to be placed along the fiber axis and 2 cm away from its epicardial end. For the whole ventricle simulations, the position of the recording electrode (x_0, y_0, z_0) was chosen approximately 3.8 cm away from the epicardial surface of the ventricular tissue volume on a transverse plane intercepting the heart at 1.85 cm from the apex.

The peaks and boundaries of pseudo-ECGs were identified using an automatic wavelet transform-based delineation system (18). The QT interval was measured between the beginning of the QRS complex and the end of the T wave. The T wave area, T_{area}, was calculated by integrating the pseudo-ECG between the beginning and end of the T wave.

Stimulation protocols

The following stimulation protocols were applied in single cell and tissue simulations. In all cases, initial conditions for the state variables of the model were determined that guaranteed convergence to a steady-state solution after prolonged pacing (>1000 stimuli) at a given frequency.

1) Periodic protocol: a train of 20 stimuli were delivered at a frequency of 1 Hz.
2) Frequency change protocol: cells / tissue were stimulated at a constant frequency of 2 Hz during 30 s, following which the frequency was changed to 0.4 Hz and stimulation continued for additional 30 s.
3) Dynamic protocol: a train of 200 stimuli was applied at a number of pacing frequencies ranging from 0.5 to 20 Hz.

For the three protocols, the stimuli were current pulses of 1-ms duration and 1.5 times diastolic threshold amplitude.

Experimental I_{Ks} current traces

Patients: Cells were prepared from 15 undiseased donor hearts. The hearts were obtained from general organ donor patients (male=7, female=8; mean age= 44.3 ± 4.3 years) undergoing pulmonary and aortic valve transplantation surgery. Before explantation of the hearts the patients did not receive any medication except for dobutamine, furosemide and plasma expanders. The experimental protocol complied with the Declaration of World Medical Association proclaimed in Helsinki and was approved by the Ethical Review Board of the Albert Szent-Györgyi Medical University (No. 51-57/1997 OEj) and by the Scientific and Research Ethical Committee of the Medical Scientific Board at the Hungarian Ministry of Health (ETT-TUKEB), under ethical approval No 4991-0/2010-1018EKU (339/PI/010).

Cell Isolation: Ventricular myocytes were isolated from the human hearts by an enzymatic dissociation procedure as described previously (19). After explantation and removal of the valves, hearts were transported to the laboratory in cold (4 °C) cardioplegic solution. A portion of the left ventricular wall was excised together with its arterial branch and was mounted on a modified 60 cm high Langendorff perfusion apparatus, where it was perfused through a branch of the left anterior descending coronary artery with solutions in the following sequence: isolation solution supplemented with 1 mM $CaCl_2$ (10 min), isolation solution (10 min), isolation solution to which collagenase (type I, 0.66 mg/ml, Sigma Chemical, St. Louis, MO, USA), elastase (type III, 0.045 mg/ml, Sigma Chemical, St. Louis, MO, USA) and bovine serum albumin (fraction V, fatty acid free, 2 mg/ml, Sigma Chemical, St. Louis, MO, USA) had been added (15 min). After the first step of enzymatic digestion, the solution was supplemented with protease (type XIV, 0.12 mg/ml, Sigma Chemical, St. Louis, MO, USA) for a further 30-45 min. Portions of the left ventricular wall that were clearly digested by the enzymes were cut into small pieces and were placed either into Kraft-Brühe (KB) solution, or into isolation solution supplemented with taurine (50 mM) and $CaCl_2$ (1.25 mM) for 15 minutes. The tissue chunks were then gently agitated in a small beaker to obtain single cells. During the entire isolation procedure, the solutions were oxygenated (100% O_2) and temperature was maintained at 37 °C. The cells were allowed to settle to the bottom of the beaker for 10 minutes, and then half of the supernatant was replaced by new solution. These procedures were repeated three times. The cells in KB solution were stored at 4 °C, and the cells stored in isolation solution (1.25 mM $CaCl_2$) were maintained on 12-14 °C. The characteristics of I_{Ks} current recorded from cells stored in KB solution did not differ from those stored in isolation solution. At least 1 hour was allowed before the start of the experiments.

Solutions used for cell isolation: The composition of the solutions was as follows (in mM): a) cardioplegic solution - NaCl 110, KCl 16, $MgCl_2$ 16, $CaCl_2$ 1.2, $NaHCO_3$ 10; b) isolation solution (Ca^{2+}-free) - NaCl 135, KCl 4.7, KH_2PO_4 1.2, $MgSO_4$ 1.2, HEPES 10, Na pyruvate 5, taurine 20, $NaHCO_3$ 4.4, Glucose 10 (pH 7.2 adjusted with NaOH); c) KB solution - KOH 90, L-glutamic acid 70, taurine 15, KCl 30, KH_2PO_4 10, $MgCl_2$ 0.5, HEPES 10, Glucose 11, EGTA 0.5 (pH 7.3 adjusted with KOH).

Experimental techniques and solutions: One drop of cell suspension was placed in a transparent recording chamber mounted on the stage of an inverted microscope (TMS Nikon Co, Tokyo, Japan) and the individual myocytes were allowed to settle to the bottom of the recording chamber for at least 5 minutes before superfusion. Only rod shaped cells, which showed clear striations, were used. Although the yield varied greatly between isolations (from 5 to 70%), the ease with which seals were formed, the stability of the seals and the quality of the measurements did not correlate with yield. Cell capacitance (182 ± 15 pF, n=19) was measured by applying 10 mV hyperpolarizing pulse from -10 mV. The holding potential was -90 mV. The capacity was measured by integration of the capacitive transient divided by the amplitude of the voltage step (10 mV). HEPES buffered Tyrode's solution was used as normal superfusate. This solution contained (mM): NaCl 144, NaH_2PO_4 0.33, KCl 4.0, $CaCl_2$ 1.8, $MgCl_2$ 0.53, Glucose 5.5, and HEPES 5.0 at pH of 7.4. Superfusion was maintained by gravity flow. E-4031 (obtained as a gift from the Institute for Drug Research, Budapest, Hungary) was prepared freshly daily as a 5 mM aqueous stock solution. Final bath concentrations of 1-5 µM E-4031 were chosen for experiments on the basis of studies showing that these concentrations completely blocked I_{Kr} in guinea pig myocytes (20). Micropipettes were fabricated from borosilicate glass capillaries (Clark, Reading, UK) using a microprocessor controlled horizontal puller (Sutter Instruments Co., Novato CA, USA) and had a resistance of 1.5 - 2.5 MOhm when filled with a solution containing (in mM) KOH 100, KCl 20, K_2HPO_4 10, $MgCl_2$ 5, K_2EGTA 5, HEPES 10, Na_2ATP 5, KADP 0.5, Na pyruvate 5, glutamate 5, creatine 5, Glucose 5. The pH of the solution was adjusted to 7.2

with aspartic acid. The external solution contained 1 μM nisoldipine (kind gift form Bayer Hungary Ltd, Budapest) in order to completely block the inward Ca^{2+} current (I_{Ca}). To increase the amplitude of I_{Ks} most of the experiments were carried out in the presence of 1 μM forskolin. The inward sodium current (I_{Na}) was inactivated by applying a holding potential of -40 mV, which largely inactivated the transient outward current (I_{to}) as well. The membrane currents were recorded with Axopatch-1D and Axopatch-200B patch-clamp amplifiers (Axon Instruments, Foster City CA, USA) using the whole-cell configuration of the patch-clamp technique. After establishing high (1-10 GOhm) resistance seals by gentle suction, the cell membrane beneath the tip of the electrode was disrupted by further suction or by applying 1.5 V electrical pulses for 1-5 ms. The series resistance was typically 4 - 8 MOhm before compensation (usually 50 - 80% depending on the voltage protocols). Those experiments in which the series resistance was high, or substantially increased during the measurements, were discarded from the analysis. The membrane currents were digitized using a 333 kHz analog-to-digital converter (Digidata 1200, Axon Instruments, Foster City CA, USA) under software control (pClamp 6.0 and 7.0, Axon Instruments, Foster City CA, USA). The results were analyzed using software programs purchased from Axon (pClamp 6.0 and 7.0, Axon Instruments, Foster City CA, USA) and were low-pass filtered at 1 kHz. The experiments were carried out at 37ºC.

Experimental APs in single myocytes

Dog and human: All AP measurements were performed at 37°C. The rod-shaped viable cells, showing clear striation, were sedimented in a lucid chamber allowing continuous superfusion with Krebs solution gassed with a mixture of 5% CO_2 and 95% O_2. Transmembrane potentials were recorded using 3 M KCl–filled sharp glass microelectrodes having a tip resistance between 20 and 40 MOhm. These electrodes were connected to the input of an Axoclamp-2B amplifier (Axon Instruments Inc., Foster City, CA). The cells were paced through the recording electrode at steady cycle length of 1000 ms using 1-ms-wide rectangular current pulses with 120% threshold amplitude. Prior to each experiment, APs were recorded for 5 min before drug application to allow the cells to equilibrate. The experiment was continued only if AP parameters remained stable during this period of time. Because the cytosol was not dialyzed, time-dependent changes in APD were negligible under these experimental conditions. When performing beat-to-beat APD variability measurements, 50 consecutive APs were recorded with a basic cycle length of 1000 ms. When the effect of dofetilide was tested, an incubation period of 5-6 minutes was applied. This incubation period was sufficient to develop the steady state drug effect. APs were digitized at 200 kHz using Digidata 1200 A/D card (Axon Instruments Inc.) and stored for later, off-line analysis.

Guinea pig: All experiments were carried out in accordance with the UK Home Office guidance on the Operation of Animals (Scientific Procedures) Act of 1986. Ventricular myocytes were enzymatically isolated from guinea pig hearts as described in detail in (21). The ventricles were then cut off at the base of the heart and bathed in high K+ solution. Tissue pieces were from the left ventricle base and apex sub-endo and sub-epicardial regions. Cells were further separated by centrifugation and pipetting. The cell membrane potential was measured with the perforated patch method. The pipette solution contained Ca^{2+} to ensure that any unintentional rupturing of the membrane would cause hyper-contraction of the cell, and its death. At membrane potentials below approximately -70 mV, a stimulus was applied (300 μs, 18 ± 2 nA) to provoke an AP. The signal was monitored using P-clamp, the sampling rate was 10 kHz, with a 5 kHz low-pass Bessel filter. The cells were paced at 1 Hz.

Experimental APs in tissue

Dog: All experiments were carried out in compliance with the *Guide for the Care and Use of Laboratory Animals* (USA NIH publication No 85-23, revised 1985). The protocols were approved by the Department of Animal Health and Food Control of the Ministry of Agriculture and Rural Development, Hungary (15.1/01031/006/2008). Adult mongrel dogs (8-16 kg) of either sex were used. Following anaesthesia (sodium pentobarbital, 30 $mg \cdot kg^{-1}$ administered intravenously), the heart of each animal was rapidly removed through right lateral thoracotomy. The hearts were immediately rinsed in oxygenated Locke's solution containing (in mM): NaCl, 120; KCl, 4; $CaCl_2$, 2; $MgCl_2$, 1; $NaHCO_3$, 22; and glucose, 11. The pH of this solution was 7.35 to 7.45 when gassed with 95% O_2 and 5% CO_2 at 37°C. To prepare midmyocardial ventricular preparations a piece from the basal part of the left ventricle was glued with tissue adhesive directly to top of the cutting stage of a vibratome (Vibratome 3000 PELCO 100 Vibratome Sectioning System). Tangential slices were cut in cold (4°C) Locke's solution with a steel blade. The slices were placed in a preincubation chamber filled with oxygenated Locke's solution at room temperature for at least 3 hours. Midmyocardial preparations were stimulated (HSE [Hugo Sachs Elektronik] stimulator type 215/II, March-Hugstetten, Germany) at a basic cycle length of 1000 ms, using 2 ms rectangular constant voltage pulses (twice diastolic threshold in intensity) isolated from ground and delivered across bipolar platinum electrodes in contact with the preparation. Each preparation was allowed to equilibrate for at least 1 hour while they were continuously superfused with Locke's solution. Temperature of the superfusate was kept constant at 37°C.
Human: Non-diseased human hearts that were technically unusable for transplantation (based on logistical, not patient-related, considerations) were obtained from general organ donors. Before cardiac explanation, organ donor patients did not receive medication except dobutamine, furosemide and plasma expanders. The investigations conform to the principles outlined in the *Declaration of Helsinki* of the World Medical Association. All experimental protocols were approved by the Scientific and Research Ethical Committee of the Medical Scientific Board at the Hungarian Ministry of Health (ETT-TUKEB), under ethical approval No 4991-0/2010-1018EKU (339/PI/010). Human cardiac tissue was stored in cardioplegic solution at 4°C for 4–8 hours. Papillary muscles were obtained from the right ventricle. Preparations were stimulated at a basic cycle length of 1000 ms and allowed at least 1 hour to equilibrate while they were continuously superfused with Locke's solution. Temperature of the superfusate was kept constant at 37°C.
Conventional microelectrode technique: Transmembrane potentials were recorded using conventional microelectrode technique as described earlier in detail (22). Microelectrodes filled with 3M KCl and having tip resistances of 5-15 MOhm were connected to the input of a high impedance electrometer (Experimetria microelectrode amplifier type 309, Budapest, Hungary), which was connected to ground. The voltage outputs from all amplifiers were displayed on a dual beam memory oscilloscope (Hitachi oscilloscope V-555, Japan). APD measured at 90% repolarization was obtained, using in house software (APES) running on an IBM compatible computer equipped with an ADA 3300 analogue-to-digital data acquisition board (Real Time Devices Inc., State College, PA, USA) having a maximum sampling frequency of 40 KHz. When beat-to-beat APD variability was measured, 50 consecutive APs were recorded with a basic cycle length of 1000 ms. The effect of dofetilide was tested after an incubation period of 60 minutes, which was sufficient to develop the steady-state drug effect.

Contribution of ion channel fluctuations to macroscopic I_{Ks} activation and deactivation variability

Panels A, B, C, and D of Fig. S1 show voltage dependence of I_{Ks} tail current amplitude, I_{Ks} activation and deactivation kinetics (obtained from fitting single exponentials to the I_{Ks}

current traces generated with the protocols described in the study by Virág et al. (23)), and normalized I_{Ks} tail current as a function of test pulse duration (to 50 mV), respectively. Simulation results including intrinsic noise only or intrinsic plus extrinsic noise are compared with experimental data (23). The values of n_{Ks} and G_{Ks} were scaled down in the simulations so as to match the maximum I_{Ks} amplitude observed in the experiments. From Fig. S1 it can be observed that, in mean, I_{Ks} properties were in general agreement between simulations and experiments. As for the variability of I_{Ks} properties, Fig. S1 shows that when only intrinsic noise was included in the stochastic model the degree of simulated variability in I_{Ks} current was well below that of the experiments, while inclusion of intrinsic plus extrinsic noise led to larger degrees of variability that were within the limits of those observed experimentally.

Temporal electrophysiological heterogeneity in cell and tissue

To assess whether the temporal APD dispersion found in simulations and experiments was related to the corresponding absolute APD values, the mean (m_{APD}) and standard deviation (σ_{APD}) of APDs over 20 consecutive cardiac cycles measured in each stochastic realization or experimental recording were quantified. From those measurements, the coefficient of variation c was evaluated as $c=(\sigma_{APD} / m_{APD}) \cdot 100$. The coefficients of variation (mean ± standard deviation) in the guinea pig simulations were c = 1.02 ± 0.17 / 1.54 ± 0.11 / 0.94 ± 0.07 for endo / mid / epi cells, while in the experimental study by Zaniboni et al. (24) the values reported for c were 2.3 ± 0.9, and in the experiments of this study c = 2.75 ± 0.84, 2.37 ± 1.05, 1.81 ± 0.62, and 2.25 ± 1.06 for apical-epi, apical-endo, basal-epi, and basal-endo cells, respectively. In the human simulations, c = 0.91 ± 0.11 / 0.98 ± 0.13 / 0.85 ± 0.10 for endo / mid / epi cells, while in the experiment of this study c = 1.28, and in the canine experiments of this study, c = 1.61 ± 0.62. In all cases, the values of c in the simulations were within the bounds of those measured in the experiments. In the simulations, the highest values of c were found for the cases with the lowest number of I_{Ks} channels in each species, as illustrated above. However, the values of c found in guinea pig were larger than those found in human, despite having a greater number of associated I_{Ks} channels. This observation, together with all our results on beat-to-beat APD variability, confirms that in each species, but not when comparing between species, channel numbers are important determinants of temporal electrophysiological heterogeneity, both when that heterogeneity is evaluated in absolute terms (as APD range over consecutive cardiac cycles) or in relative terms (as coefficient of variation).

Quantification of beat-to-beat APD variability in relative terms using the coefficient of variation c also confirmed that coupling mitigated the temporal manifestation of ion channel fluctuations at the tissue level. In simulations, mean values of c in guinea pig endo / mid / epi cells changed from 1.02 / 1.54 / 0.94 before coupling to 0.23 / 0.17 / 0.25 after coupling. In experiments, a reduction in c from 2.3 to 1.5 due to coupling was reported in a subset of the recordings analyzed by Zaniboni et al. (24). In human simulations, coupling acted to reduce the coefficient of variation c in endo / mid / epi cells from 0.91 / 0.98 / 0.85 to 0.16 / 0.14 / 0.17. In human experiments, c changed from 1.28 to 0.44, and in dog experiments from 1.61 to 0.31.

Manifestation of I_{Ks} stochasticity in pseudo-ECGs

Beat-to-beat variability computed from 20 successive beats paced at 1 Hz was quantified for QT and T_{area}. Fig. S4A and Fig. S4B (top left panel) show the 20 superimposed pseudo-ECGs corresponding to a representative stochastic realization at normal coupling (black line) in guinea pig and human, respectively. Also shown in those panels are representations for simulated I_{Kr} block (gray line), which will be described and discussed below. Additionally, Fig. S4A and Fig. S4B (top middle and right panels) present the averaged ranges, over

realizations, covered by QT and T_{area} along the 20 successive beats for reduced, normal, and enhanced coupling (black boxes). The bottom panels of Fig. S4A and Fig. S4B show three Poincaré plots representing the QT interval of the n-th beat versus the QT interval of the (n-1)-th beat for the three simulated degrees of coupling (black dots in each plot). The first observation from the bar graphs shown in Fig. S4 is that temporal variability in the pseudo-ECG was of very low magnitude under control conditions. At normal coupling, the QT interval changed over time by 0.6 ms in guinea pig, and by 2.0 ms in human. Also, T_{area} presented very little variations: 1.0 and 1.8 mVms, respectively. Enhanced coupling did not practically alter temporal variability of the ECG indices (0.7 and 2.0 ms for QT, and 1.0 and 1.7 mVms for T_{area}). On the other hand, reduced coupling acted to slightly unmask temporal fluctuations in the pseudo-ECG (0.7 and 2.1 ms for QT, and 1.0 and 2.2 mVms for T_{area}). This is confirmed by the results of the QT Poincaré plots, where dots are accumulated around the diagonal in all cases.

When variability was evaluated for the two analyzed ECG indices following I_{Kr} block, increases in their temporal ranges of 526% for the QT interval and 109% for T_{area} in guinea pig, and 43% and 35% in human, respectively, were found in physiologically coupled tissue. This is illustrated in Fig. S4A and Fig. S4B (gray line). A comparison of the Poincaré plots shown in those figures confirmed that, in guinea pig, instabilities were generated under reduced coupling following I_{Kr} block. In human, instabilities could not be observed, but deviations of the points from the diagonal became more pronounced under those conditions, although very moderately. These observations are in agreement with results shown in experimental and clinical studies that have investigated drug-induced or disease-related instabilities and its relation to proarrhythmia (25,26).

I_{Ks} stochasticity and the genesis of APD alternans

I_{Ks} current fluctuations also facilitate the occurrence of APD alternans. The frequency threshold for APD alternans was found to be notably lowered after introducing stochastic I_{Ks} fluctuations into the deterministic models (Fig. S5). Specifically, under control conditions, the threshold for APD alternans in isolated epi cells decreased from 16.67 Hz (deterministic) to 10 Hz (stochastic) in guinea pig, and from 4.55 to 4 Hz in human. Under I_{Kr} block, the threshold was reduced from 14.29 Hz (deterministic) to 8.70 Hz (stochastic) in guinea pig, and from 3.33 to 2.22 Hz in human, respectively. In mid cells, which present larger degrees of temporal variability, APD alternans were more easily induced (not shown), with frequency thresholds being 6.25 and 2.50 Hz in stochastic guinea pig and human models under control, and 4.76 and 1.67 Hz under I_{Kr} block. Those observations confirmed the role of I_{Ks} ion channel fluctuations in modulating APD alternans, particularly under I_{Kr} block conditions.

References for Supporting Material

1. Lu, Z., K. Kamiya, T. Opthof, K. Yasui, and I. Kodama. 2001. Density and kinetics of I(Kr) and I(Ks) in guinea pig and rabbit ventricular myocytes explain different efficacy of I(Ks) blockade at high heart rate in guinea pig and rabbit: implications for arrhythmogenesis in humans. Circulation. 104:951-956.
2. Hoppe, U. C., E. Marbán, and D. C. Johns. 2001. Distinct gene-specific mechanisms of arrhythmia revealed by cardiac gene transfer of two long QT disease genes, HERG and KCNE1. Proc. Natl. Acad. Sci. USA. 98:5335–5340.
3. Li, G. R., C. P. Lau, T. K. Leung, and S. Nattel. 2004. Ionic current abnormalities associated with prolonged action potentials in cardiomyocytes from diseased human right ventricles. Heart Rhythm 1:460-468.

4. Jost, N., L. Virág, M. Bitay, J. Takács, C. Lengyel, P. Biliczki, Z. Nagy, G. Bogáts, D. A. Lathrop, J. G. Papp, and A. Varró. 2005. Restricting excessive cardiac action potential and QT prolongation: a vital role for IKs in human ventricular muscle. Circulation. 112:1392–1399.
5. Sanguinetti, M. C., and N. K. Jurkiewicz. 1990. Two components of cardiac delayed rectifier K+ current. Differential sensitivity to block by clas III antiarrhythmic agents. J. Gen. Physiol. 96:195-215.
6. Levi, A. J. 1991. The effect of strophanthidin on action potential, calcium current and contraction in isolated guinea-pig ventricular myocytes. J. Physiol. 443:1-23.
7. Linz, K. W., and R. Meyer. 1998. Control of L-type calcium current during the action potential of guinea-pig ventricular myocytes. J. Physiol. 513:425-442.
8. Williams, B. A., D. R. Dickenson, and G. N. Beatch. 1999. Kinetics of rate-dependent shortening of action potential duration in guinea-pig ventricle; effects of IK1 and IKr blockade. Br. J. Pharmacol. 126:1426-1436.
9. Terrar, D. A., C. M. Wilson, S. G. Graham, S. M. Bryant, and B. M. Heath. 2007. Comparison of guinea-pig ventricular myocytes and dog Purkinje fibres for in vitro assessment of drug-induced delayed repolarization. J. Pharmacol. Toxicol. Methods 56:171-185.
10. Li, G. R., J. Feng, L. Yue, M. Carrier, and S. Nattel. 1996. Evidence for two components of delayed rectifier K+ current in human ventricular myocytes. Circ. Res. 78:689-696.
11. Li, G.R., B. Yang, J. Feng, R. F. Bosch, M. Carrier, and S. Nattel. 1999. Transmembrane ICa contributes to rate-dependent changes of action potentials in human ventricular myocytes. Am. J. Physiol. 276:H98-H106.
12. Glukhov, A. V., V. V. Fedorov, Q. Lou, V. K. Ravikumar, P. W. Kalish, R. B. Schuessler, N. Moazami, and I. R. Efimov. 2010. Transmural dispersion of repolarization in failing and nonfailing human ventricle. Circ. Res. 106:981-991.
13. ten Tusscher, K. H., and A. V. Panfilov. 2006. Alternans and spiral breakup in a human ventricular tissue model. Am. J. Physiol. Heart Circ. Physiol. 291:H1088-H1100.
14. Gima, K., and Y. Rudy. 2002. Ionic current basis of electrocardiographic waveforms: a model study. Circ. Res. 90:889-896.
15. Bishop, M. J., G. Plank, R. A. Burton, J. E. Schneider, D. J. Gavaghan, V. Grau, and P. Kohl. 2010. Development of an anatomically detailed MRI-derived rabbit ventricular model and assessment of its impact on simulations of electrophysiological function. Am. J. Physiol. Heart Circ. Physiol. 298:H699–H718.
16. Bueno-Orovio, A., E. M. Cherry, and F. H. Fenton. 2008. Minimal model for human ventricular action potentials in tissue. J. Theor. Biol. 253:544–560.
17. Pitt-Francis, J., M. O. Bernabeu, J. Cooper, A. Garny, L. Momtahan, J. Osborne, P. Pathmanathan, B. Rodríguez, J. P. Whiteley, and D. J. Gavaghan. 2008. Chaste: using agile programming techniques to develop computational biology software. Philos. Trans. A Math. Phys. Eng. Sci. 366:3111–3136.
18. Martínez, J. P., R. Almeida, S. Olmos, A. P. Rocha, and P. Laguna. 2004. A wavelet-based ECG delineator: evaluation on standard databases. IEEE Trans. Biomed. Eng. 51:570-581.
19. Iost, N., L. Virág, M. Opincariu, J. Szécsi, A. Varró, and J. G. Papp. 1998. Delayed rectifier potassium current in undiseased human ventricular myocytes. Cardiovasc. Res. 40:508-515.
20. Sanguinetti, M. C., and N. K. Jurkiewicz. 1990. Two components of cardiac delayed rectifier K+ current. Differential sensitivity to block by clas III antiarrhythmic agents. J. Gen. Physiol. 96:195-215.

21. Iribe, G., M. Helmes, and P. Kohl. 2006. Force-length relations in isolated intact cardiomyocytes subjected to dynamic changes in mechanical load. Am. J. Physiol. Heart Circ. Physiol. 292:H1487-H1497.
22. Varró, A., B. Baláti, N. Iost, J. Takács, L. Virág, D. A. Lathrop, C. Lengyel, L. Tálosi, and J. G. Papp. 2000. The role of the delayed rectifier component I_{Ks} in dog ventricular muscle and Purkinje fibre repolarisation. J. Physiol. 523:67-81.
23. Virág, L., N. Iost, M. Opincariu, J. Szolnoky, J. Szécsi, G. Bogáts, P. Szenohradszky, A. Varró, and J. G. Papp. 2001. The slow component of the delayed rectifier potassium current in undiseased human ventricular myocytes. Cardiovasc. Res. 49:790-797.
24. Zaniboni, M., A. E. Pollard, L. Yang, and K. W. Spitzer. 2000. Beat-to-beat repolarization variability in ventricular myocytes and its suppression by electrical coupling. Am. J. Physiol. Heart Circ. Physiol. 278:H677-H687.
25. Hondeghem, L. M., L. Carlsson, and G. Duker. 2001. Instabiliy and triangulation of the action potential predict serious proarrhythmia, but action potential duration prolongation is antiarrhythmic. Circulation. 103:2004–2013.
26. Hinterseer, M., B. M. Beckmann, M. B. Thomsen, A. Pfeufer, M. Ulbrich, M. F. Sinner, S. Perz, H. E. Wichmann, C. Lengyel, R. Schimpf, S. K. Maier, A. Varró, M. A. Vos, G. Steinbeck, and S. Kääb. 2010. Usefulness of short-term variability of QT intervals as a predictor for electrical remodeling and proarrhythmia in patients with nonischemic heart failure. Am. J. Cardiol. 106:216-220.
27. Bryant, S. M., X. Wan, S. J. Shipsey, and G. Hart. 1998. Regional differences in the delayed rectifier current (IKr and IKs) contribute to the differences in action potential duration in basal left ventricular myocytes in guinea-pig. Cardiovasc Res 40:322–331.
28. Li, G. R., J. Feng, L. Yue, and M. Carrier. 1998. Transmural heterogeneity of action potentials and Ito1 in myocytes isolated from the human right ventricle. Am. J. Physiol. 275:H369-H377.

Figure legends for Supporting Material

Figure S1: Mean ± standard error (SE) of human I_{Ks} tail current amplitude (panel A), activation (B) and deactivation (C) kinetics, and normalized tail current (D), obtained from simulations and experiments (23) using the same voltage protocols. For the simulations, n_{Ks} and G_{Ks} have been scaled to match the maximum I_{Ks} amplitude of the experiments. Results shown in left panels correspond to simulations that contain intrinsic noise only, while those in middle panels include intrinsic plus extrinsic noise.

Figure S2: Simulated and experimental beat-to-beat APD variability in guinea pig (A) and human (B) ventricular myocytes, from endocardium, midmyocardium, and epicardium, under steady-state pacing at 1 Hz (except for experiments of (24) where pacing is at 0.5 Hz). Each line represents one of the 20 simulated beats.

Figure S3: Cell-to-cell APD variability. (A) APD values (mean ± SE) from experimental and simulated guinea pig myocytes during steady-state pacing at 1 Hz (n=15 for simulations, n=10, 11 for experiments of this study, and n=24, 25, 24 for experiments of (27)). (B) Analogous results in human (n=15 for simulations, n=1 for experiment of this study, and n=15, 21, 19 for experiments of (28)).

Figure S4: ECG variability. Top left panel: simulated ECG traces obtained from 20 consecutive cardiac cycles at 1 Hz steady-state pacing for guinea pig (A) and human (B), under control (black line) and full I_{Kr} block (gray line). Top middle and right panels: maximal

beat-to-beat variability in QT interval, and T wave area under simulated reduced, normal and enhanced coupling. Bottom panel: QT Poincaré plots for the three coupling cases.

Figure S5: APD alternans. (A) Top panel: threshold frequency for APD alternans in guinea pig epi cells under control and I_{Kr} block. Bottom panel: APD alternans occurring in an epi guinea pig myocyte simulated with the stochastic model, but not for the one simulated with the deterministic model, under 10 Hz pacing for control, and 8.70 Hz for I_{Kr} block. (B) Analogous results for human, where represented APD alternans are obtained with the stochastic epi model after pacing at 4 Hz for control, and 2.22 Hz for I_{Kr} block.

Figure S6: Potential effects of larger simulated I_{Ks} noise levels on APD variability and arrhythmogenesis in guinea pig (A) and human (B), under control and following I_{Kr} block. Left panel: beat-to-beat APD variability ranges in epi cells paced at 1 Hz as a function of the scaling factor ρ applied to the number of I_{Ks} channels (for each value of ρ, the number of I_{Ks} channels in the AP model is ρ times the default n_{Ks} value provided in the text, while G_{Ks} is kept constant for the four simulated cases). Middle panel: percentage of epi cells showing EADs after suddenly changing pacing rate from 1 to 0.4 Hz, represented as a function of the scaling factor ρ. Right panel: frequency thresholds for APD alternans in epi cells as a function of the scaling factor ρ.

Fig. S1: IKs properties

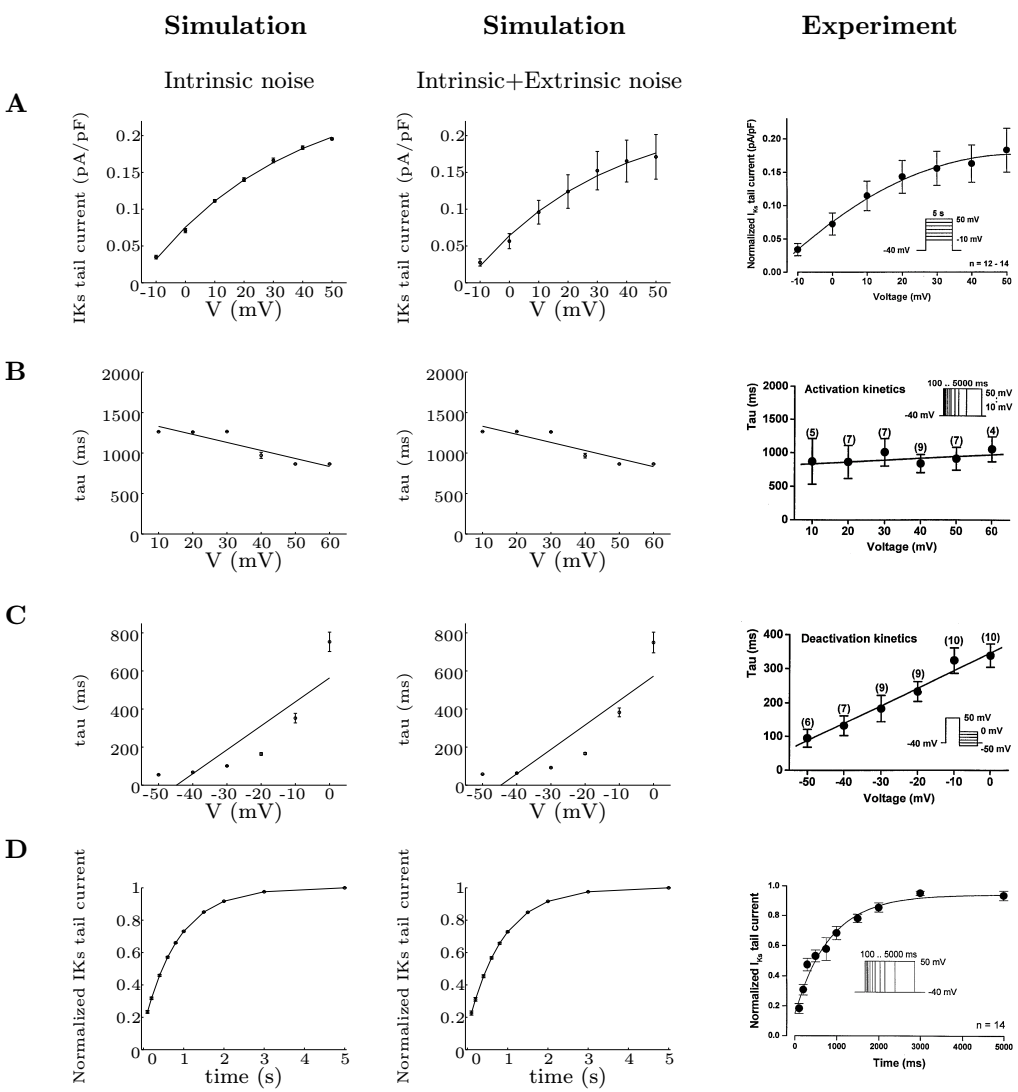

Virag et al., 2001

Fig. S2: Beat-to-beat APD variability

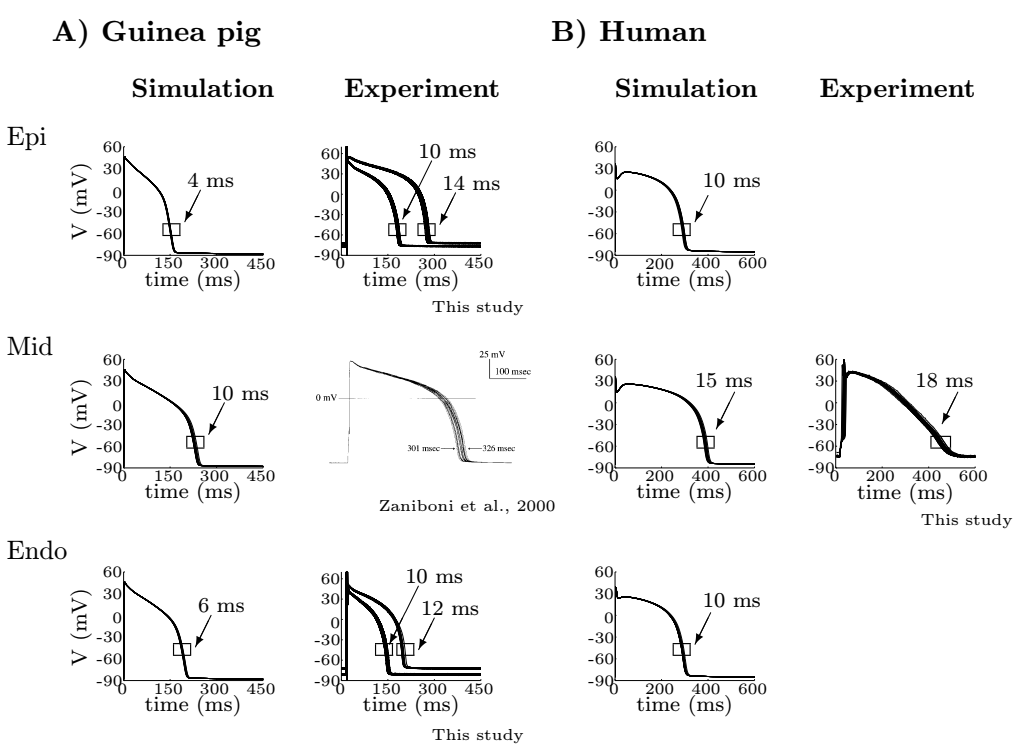

Fig. S3: Cell-to-cell APD variability

A) Guinea pig

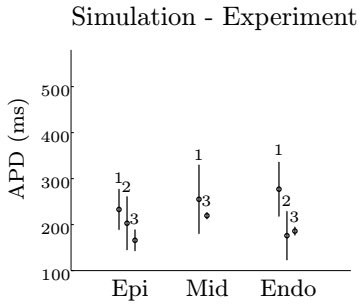

1) Bryant et al., 1998
2) Experiments of this study
3) Simulation, stoch. FR07

B) Human

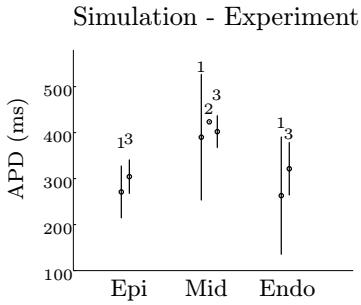

1) Li et al., 1998
2) Experiment of this study
3) Simulation, stoch. TP06

Fig. S4: ECG variability

A) Guinea pig

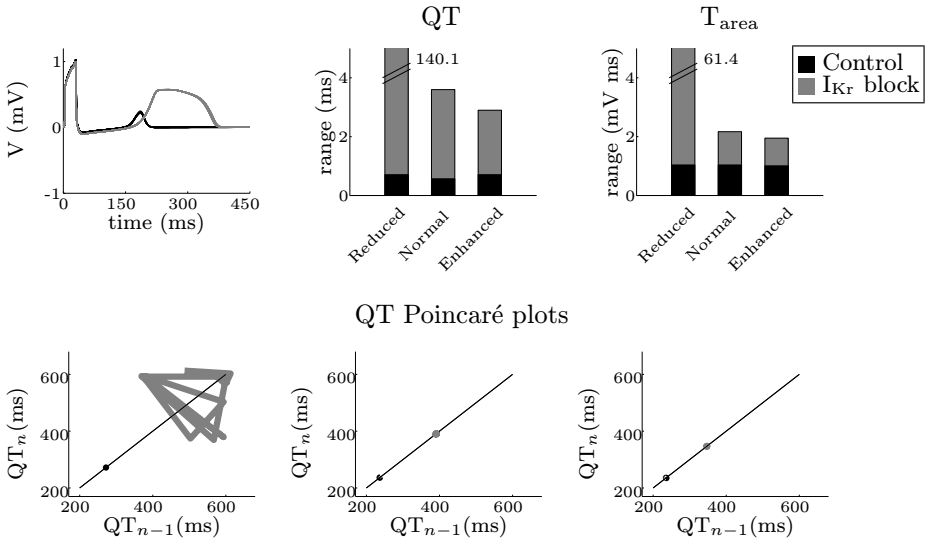

B) Human

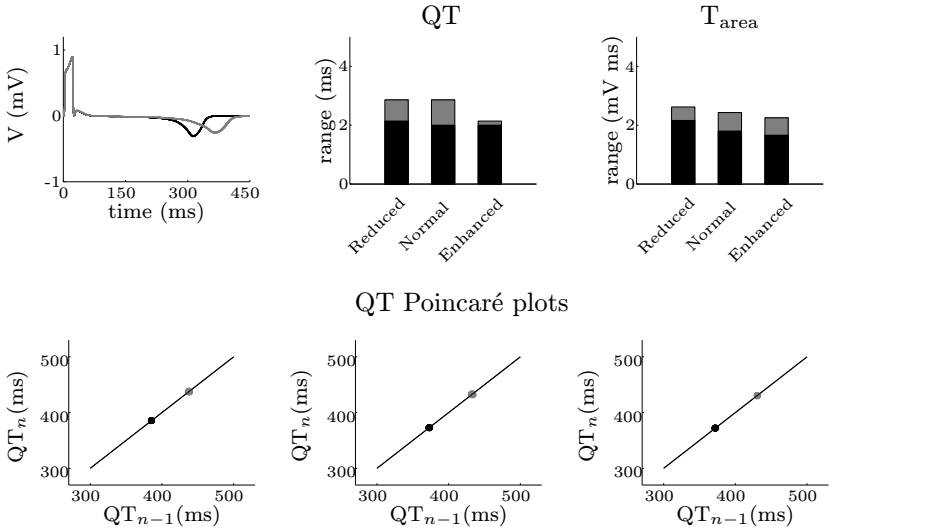

Fig. S5: APD alternans

A) Guinea pig

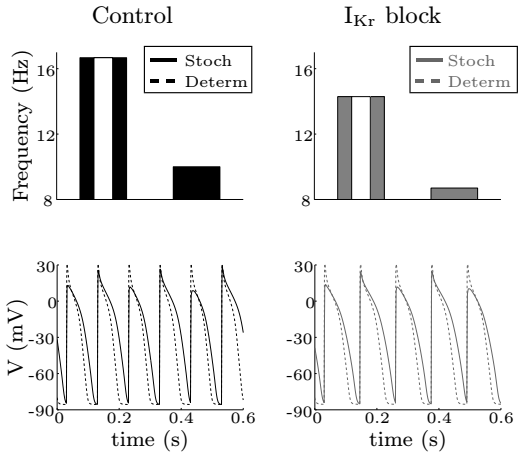

B) Human

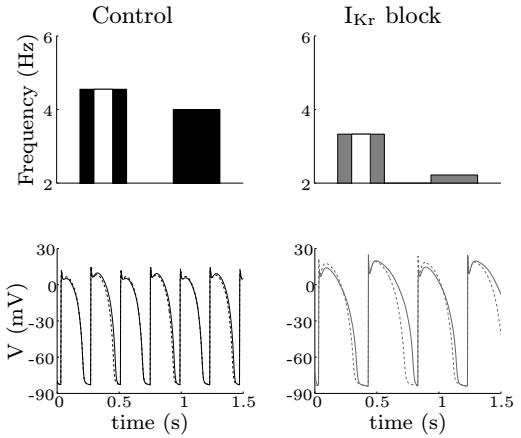

Fig. S6: Effects of larger IKs noise levels

A) Guinea pig

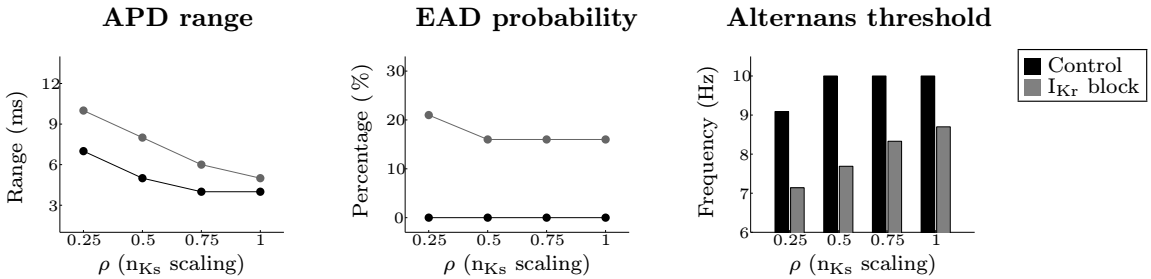

B) Human